Modeling the Magnetic Ordering of Magnetite (Fe_3O_4) Nanoparticle Assemblies

Brittni Newbold Pratt

A senior thesis submitted to the faculty of
Brigham Young University
in partial fulfillment of the requirements for the degree of

Bachelor of Science

Dr. Karine Chesnel, Advisor

Department of Physics and Astronomy

Brigham Young University

ABSTRACT

Modeling the Magnetic Ordering of Magnetite (Fe_3O_4) Nanoparticle Assemblies

Brittni Newbold Pratt
Department of Physics and Astronomy, BYU
Bachelor of Science

Magnetite nanoparticles have great potential for use in medical and other applications, so understanding their properties is crucial. A property still left to be understood is the magnetic ordering of assemblies of nanoparticles at the nanoscale. This paper addresses how the magnetic ordering in magnetite nanoparticle assemblies changes as a function of nanoparticle size and external magnetic field at high temperature. Nanoparticle assemblies were fabricated using organic methods and placed on membranes. These samples were put through x-ray resonant magnetic scattering (XRMS) which produced scattering images that provided information about the magnetic ordering of the particles. Various images were obtained using XRMS for different field values and temperatures. These images were reduced to one-dimensional scattering profiles. By fitting these scattering profiles with a model, we found the percentages of ferromagnetic contribution, antiferromagnetic contribution, and the random contribution. There is a large random contribution as the field value approaches 0 Oe for Sample 9, the sample with the smallest particles, at 300 K. For Sample 3, the sample with the largest particles, at 280 K and at 300 K, there is a slight increase in the antiferromagnetic contribution and large random contribution at low field value. The larger particles are thus demonstrating more antiferromagnetic ordering at low magnetic field values than the smaller particles when placed in high temperature. Therefore, our methods yield information about the magnetic ordering of magnetite nanoparticles and the possibility to control the magnetic ordering through particle size.

Keywords: Magnetite nanoparticles, magnetic ordering, XRMS, scattering profiles

ACKNOWLEDGMENTS

I would like to express my gratitude for my research advisor, Dr. Karine Chesnel. Participating in this research project has been an incredible experience for me because of her support and patience. I am also grateful to my wonderful husband and daughter, Chris and Madison, who always encourage me and support me.

Contents

Table of Contents **iv**

List of Figures **vi**

1 Introduction **1**
1.1 Motivation 1
1.2 Magnetic Properties of Magnetite Nanoparticles 2
1.3 Previous Work at BYU 4
1.4 Overview 5

2 Fabrication of the Nanoparticles **6**
2.1 Overview of the Fabrication 6
2.2 Determining Particle Size and Distribution 8

3 Synchrotron Experiment and Data **11**
3.1 Synchrotron Experiment 11
3.2 Estimation of Interparticle Distance from the XRMS Profiles 12
3.3 Magnetic and Dichroic Ratios 14

4 Magnetic Order Modeling of Nanoparticles **17**
4.1 Modeling a Chain of Nanoparticles and Magnetic Ordering 17
4.2 Modifications to Previous Model 20
4.2.1 Modeling Spatial Distance between Particles 21
4.2.2 Flattening Technique 21
4.2.3 Constraining Sigma Values 21
4.2.4 Modeling the Magnetic and Dichroic Ratios 22
4.2.5 Creating a Global Fit 22
4.3 Automating the Code using Julia 23

5 Results and Discussion **25**
5.1 Sample 9 at 300 K 25
5.2 Sample 3 at 300 K 27

5.3 Sample 3 at 280 K 29
5.4 Discussion of Results 30
5.5 Conclusion 31
5.6 Future Outlook 31

Appendix A Model Fits 32

Appendix B MATLAB Code 39
B.1 Importing Data 39
B.2 Modeling Code 43
B.3 Generating Coefficient Maps 52

Bibliography 54

Index 56

List of Figures

1.1 Superparamagnetism in Magnetite Nanoparticles 3

2.1 Setup for Nanoparticle Fabrication 7

2.2 Nanoparticle Solution NP25 and NP26 8

2.3 TEM Images of NP16, NP17, and NP18 9

2.4 TEM Image of NP25 10

2.5 TEM Image of NP26 10

3.1 Synchrotron Experimental Setup 12

3.2 One-dimensional Representations 13

3.3 Dichroic and Magnetic Ratios 16

4.1 Nanoparticle Chain Model 18

4.2 Fourier Transforms 19

4.3 Global Fits 22

5.1 Sample 9 at 300 K All Field Values 26

5.2 Sample 9 at 300 K Coefficient Map 26

5.3 Sample 3 at 300 K All Field Values 28

5.4 Sample 3 at 300 K Coefficient Map 28

5.5 Sample 3 at 280 K All Field Values 29
5.6 Sample 3 at 280 K Coefficient Map 30

A.1 Model Fits for Sample 9 at 300 K 33
A.2 Model Fits for Sample 9 at 300 K 34
A.3 Model Fits for Sample 3 at 300 K 35
A.4 Model Fits for Sample 3 at 300 K 36
A.5 Model Fits for Sample 3 at 280 K 37
A.6 Model Fits for Sample 3 at 280 K 38

Chapter 1

Introduction

This chapter introduces and provides the motivation for the topic of this thesis, which is studying the magnetic ordering of magnetite nanoparticles. Section 1.2 explains the properties of magnetite nanoparticles. The previous work done by members of this research group is then reviewed in section 1.3. The chapter concludes by giving an overview of the thesis.

1.1 Motivation

Nanoparticles have become a topic of interest for scientists today because of their many applications in medical and other fields. Since the synthesis of the nanoparticles can be varied to control the resulting shapes and sizes, they can be utilized in many ways. The optical properties of nanoparticles also make them good candidates for applications in biomedical imaging, sunglasses and heat mirror films [1, 2]. Scientists have also studied magnetic nanoparticles with hopes of improving agriculture through nanopesticides and for targeting drug delivery [3, 4].

Magnetite nanoparticles are of special interest because they align in the presence of an external magnetic field. This property makes them especially useful in magnetic resonance imaging because their ability to align increases the image contrast allowing for more accurate detection of objects like tumors [5]. Their ability to align is also particularly useful for other medical applications like drug targeting. Much has been learned through studying magnetite nanoparticles, but there is still a lot left to discover about them. Magnetite nanoparticles have great potential for success in the applications mentioned, so it is crucial that we understand their properties.

The goal of this project is to learn how the magnetic ordering in nanoparticle assemblies varies depending on nanoparticle size, temperature, and strength of the magnetic field they are placed in. Understanding these changes shows whether or not the magnetic ordering can be controlled based on these parameters. Another goal of this project is to find the best method of preparation for magnetite nanoparticles that yields uniform size distribution. Having a greater understanding of how to control the magnetic ordering of the particles when self-assembled yields fruitful results in medical and other applications. The following section discusses the magnetic properties of magnetite nanoparticles.

1.2 Magnetic Properties of Magnetite Nanoparticles

Magnetite is made up of iron ions that create a net magnetization in a magnetite nanoparticle. Fe_3O_4 is composed of Fe^{3+} and Fe^{2+} ions which have different magnitudes of spin and align in a ferrimagnetic way throughout the spinel crystallographic structure [6]. This ferrimagnetic arrangement creates a net magnetic moment at the scale of the nanoparticle. This net magnetization is called a "nanospin".

The orientation of the nanospins is dependent upon the external magnetic field that they are placed in. A demonstration of this is given in Fig. 1.1. In the absence of an external magnetic field, the nanospins (represented by the blue arrows) are oriented randomly resulting in zero net magnetization (see Fig. 1.1(a)). When an external magnetic field (represented by the red arrows) is applied to a group of these particles, the nanospins tend to align with the field which maximizes

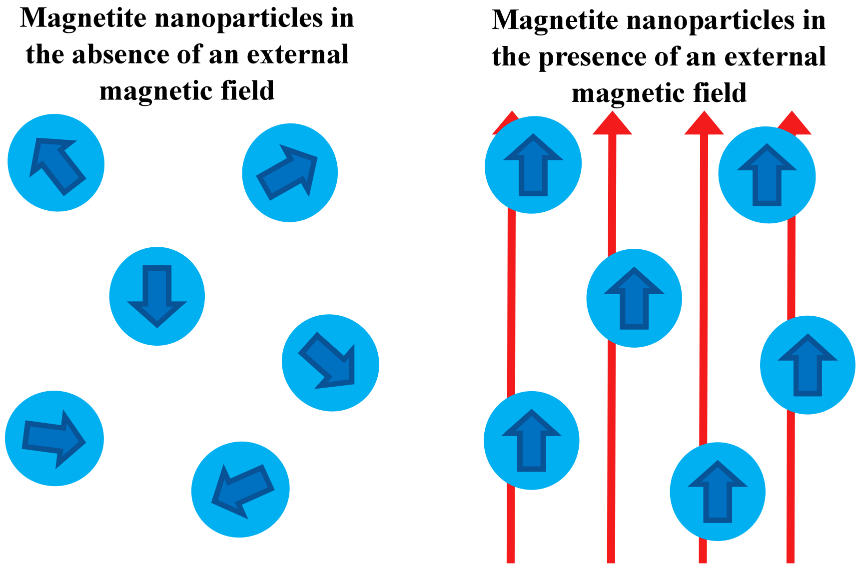

(a) (b)

Figure 1.1 Magnetite nanospins (blue arrows) are (left) randomly aligned in the absence of an external magnetic field and (right) align with the external magnetic field (red arrows) when present.

the net magnetization of the material (see Fig. 1.1(b)). This property is called superparamagnetism and is a fundamental characteristic of magnetite nanoparticles [7]. A study performed by Chang-Neg Shauo et al. [2] shows how magnetite nanoparticles displayed perfect superparamagnetism above a certain temperature, known as the blocking temperature. Their study included magnetite nanoparticles varying in size, and the blocking temperature of the particles depended on particle size and separation distance. Karine Chesnel et al. [8] also conducted a study showing drastic changes in the blocking temperature, when particle size increases from 5 to 11 nm. In this study, they also show magnetization loops for magnetite nanoparticles at varying temperatures. These magnetization loops demonstrated superparamagnetic behavior at high temperature.

The alignments of groups of nanoparticles lead to different magnetic orders. When a group of nanoparticles all align in the same direction, referred to as "ferromagnetic ordering" at the nanoscale, it produces a large net magnetization. On the other hand, if the nanospins align antiparallel, referred to as "antiferromagnetic ordering" at the nanoscale, the net magnetization becomes nearly zero on average. When there is a lack of ordering among the nanoparticles, meaning there is not a pattern in the way the nanospins are aligned, this is referred to as random ordering. The net magnetization from random ordering also averages to zero.

1.3 Previous Work at BYU

This study began in 2013 when three batches of nanoparticles were created [9]. These batches were labeled NP16, NP17, and NP18. NP16 is made of the largest particles, about 11 nm in diameter, and NP18 is made of the smallest particles, about 5 nm in diameter. From each of these batches, three samples with different concentrations were made. Samples 1-3 are from NP16, Samples 4-6 are from NP17, and Samples 7-9 are from NP18. This paper focuses on results from Sample 3 and Sample 9. The fabrication of the nanoparticles is explained in greater detail in Ch. 2. These nanoparticles were then taken to the Stanford Linear Accelerator Center (SLAC) synchrotron and scattering images were obtained through x-ray resonant magnetic scattering (XRMS). Section 3.1 describes the details of this experiment.

Dalton Griner, a previous group member, obtained one-dimensional profiles for the magnetic and dichroic ratios of the samples from the scattering images. Sections 3.2 and 3.3 review how these profiles were obtained. The magnetic and dichroic ratios provided information about the magnetic signal of the nanoparticles [9]. This information can help us understand the magnetic ordering of the nanoparticles.

Dallin Smith, another previous group member, created a base MATLAB code to model the profiles. His work included creating an array which represented a chain of nanoparticles whose magnetic ordering could be adjusted, allowing us to fit the experimental data [10]. This model is discussed in greater detail in Sec. 4.1. My work in this study is focused on making refinements to this code to find how to most accurately model the nanoparticles and to use this model to fit the data.

1.4 Overview

This thesis addresses the procedures taken to determine the magnetic ordering of the nanoparticle assemblies for Sample 9 at 300 K and Sample 3 at 300 K and at 280 K. Chapter 2 discusses the fabrication methods for the nanoparticle assemblies used in this study. This section also describes the fabrication methods attempted while trying to obtain larger nanoparticles. The techniques used to determine the particle size distribution is then explained. Next, chapter 3 gives a review of the synchrotron experiment in which the nanoparticle assemblies underwent XRMS and scattering images were obtained. One-dimensional representations of the data were then used to acquire magnetic and dichroic ratios that give information about the magnetic signal. Finally, chapter 4 explains the modeling process used to fit the magnetic ratios and determine the weight that each magnetic order contributes to the magnetic signal in the samples. Additionally, this chapter covers modifications made to the model discussed in section 1.3.

Our results and the future goals for this project are addressed in Ch. 5. Since my work was primarily on modeling Sample 9 at 300 K and Sample 3 at 300 K and at 280 K, this chapter focuses on the results from those samples. My results show that for Sample 9 at 300 K and Sample 3 at 300 K and at 280 K, there is mostly random ordering as we decrease the field value to zero; the fits from Sample 3 at 300 K and at 280 K show a small peak in the antiferromagnetic order at low field value. To more precisely determine how temperature and nanoparticle size affects the magnetic ordering of the nanoparticle assemblies, future studies will include the modeling of the remaining samples and implementation of error bars for the uncertainty.

Chapter 2

Fabrication of the Nanoparticles

This chapter discusses the fabrication of the three batches of nanoparticles used in this study, NP16, NP17, and NP18. It also reviews the procedures taken to create new batches of nanoparticles, which were called NP25 and NP26. The last section covers the methods used to image and analyze these batches.

2.1 Overview of the Fabrication

The nanoparticles used in this study, NP16, NP17, and NP18, were fabricated using organic methods [9]. To create NP16, an iron (III) oleate was mixed with oleic acid and octadecene. The solution was then heated to 320° C, kept at that temperature for 30 min, precipitated with ethanol and isolated through centrifugation. NP17 was fabricated by mixing an iron (III) acetylacetonate precursor with hexadecene, octadecene, oleic acid, and oleylamine. The resulting solution was heated to 200° C, kept at that temperature for 30 min, precipitated with ethanol and isolated through centrifugation. NP18 was created using the same method as NP17 except with diphenyl ether instead of octadecene. Different concentrations of the nanoparticles from these batches were deposited on nine silicon nitrite membranes attempting to form monolayers of the particles. They were labeled as

Samples 1-9. Samples 1-3 came from NP16, Samples 4-6 came from NP17, and Samples 6-9 came from NP18.

Figure 2.1 Heating mantle where the nanoparticles were held at 312° C for 30 min.

For use in future studies, I fabricated a new batch of nanoparticles, NP25, by using the organic method done in a study by Jongham Park et al. [11]. I created an iron oleate by mixing iron chloride, ethanol, distilled water, and hexane and heating it in an oil bath at 70° C for 4 hours. The organic layer was then isolated and magnesium sulfate was used as a drying agent. I then filtered the solution and evaporated the hexane using a rotary evaporator. The remaining solution was red and oily. This iron oleate was combined with oleic acid and octadecene, heated to 312° C, and held there for 30 min. Fig. 2.1 shows the nanoparticle solution in the heating mantle and the thermometer that allowed the solution's temperature to be monitored for 30 min. I then precipitated the solution with ethanol, centrifuged it, and decanted it. As can be seen on the left in Fig. 2.2, this remaining solution was dark and oily. The nanoparticle solution was dissolved in chloroform in three different concentrations and deposited on three ultra-thin carbon membranes.

I also created another batch of nanoparticles, NP26 for TEM imaging purposes. I followed the same procedure described in the previous paragraph using hexadecene instead of octadecene.

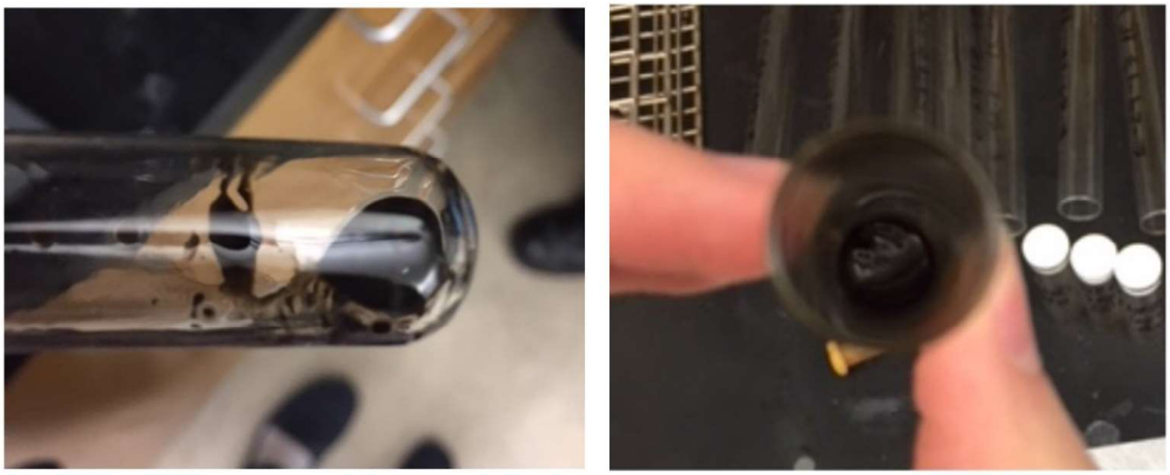

Figure 2.2 Nanoparticle solutions NP25 (left) and NP26 (right) after being centrifuged and decanted.

Since the boiling point of hexadecene is lower than that of octadecene, this solution was only heated to 275° C, and held it there for 30 min. The solution was black and very wet, but became pasty with centrifugation (See right image in Fig. 2.2). This nanoparticle solution was also dissolved in chloroform in different concentrations and deposited on ultra-thin carbon membranes.

2.2 Determining Particle Size and Distribution

Transmission Electron Microscopy (TEM) was used to image the nanoparticles and to find the size and the distribution of the nanoparticles. TEM allows high-resolution images by sending a beam of electrons through the material, which scatters them. The electrons are then gathered to produce an image of the material. Once TEM images of our nanoparticles were obtained, we analyzed them using an image processing program called ImageJ. Through ImageJ, we circled each particle in the image and obtained an average diameter for the particles.

TEM and ImageJ both indicated various particle size and distribution for NP16, NP17, and NP18. The upper plots in Fig. 2.3 show the TEM images of NP16, NP17, and NP18 from left to

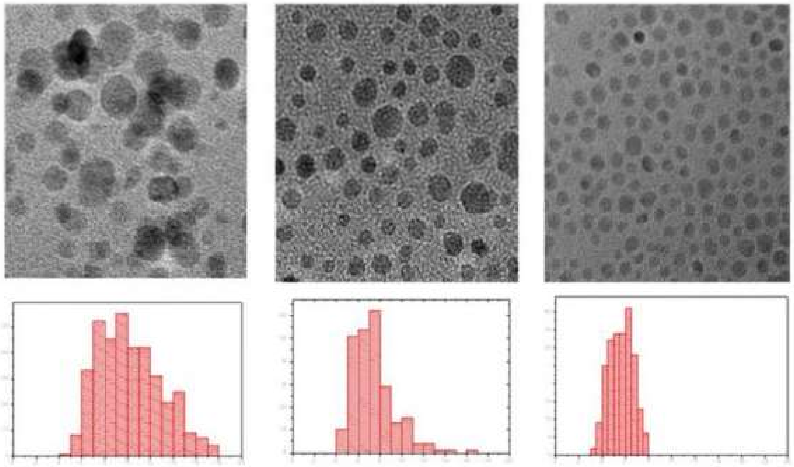

Figure 2.3 TEM images of NP16, NP17, and NP18 from left to right. Distribution graphs of particle diameter are also shown below the images. Figure taken from Griner's senior thesis [9, 12]

.

right. The nanoparticles, especially the smaller ones in NP18, tend to self-assemble in a hexagonal lattice. The images were then analyzed using ImageJ; the average diameter of the nanoparticles in each sample are shown in Table 2.1 [9]. The distribution of the diameters is shown in the lower plots of Fig. 2.3.

Table 2.1 The radii of NP16, NP17, NP18, NP25, and NP26 [9].

Batch	Diameter (nm)
NP16	11.3 ± 2.5
NP17	8.1 ± 1.7
NP18	5.6 ± 1
NP25	13.2 ± 6
NP26	14 ± 5

I used these same techniques to determine the size and distribution of NP25 and NP26. A

TEM image and distribution of the particles' diameters for NP25 is shown in Fig. 2.4. As shown, the nanoparticles are not very uniform in size, and a histogram of the particle size shows how the diameters cluster around two different radii: 6 nm and 17.5 nm. The clustering around two different radii could be due to the length of time the solution was held at 312° C or lack of sufficient centrifugation. NP26 was created in an attempt to isolate larger nanoparticles and achieve more uniform size. TEM images of NP26 were hard to achieve and analyze due to the density of the nanoparticle solution; though the solution was very dense, the images show very few nanoparticles (See Fig. 2.5). This result is mostly likely due to an error made during the fabrication; the methods used to create NP26 should be attempted again in the future for comparison purposes.

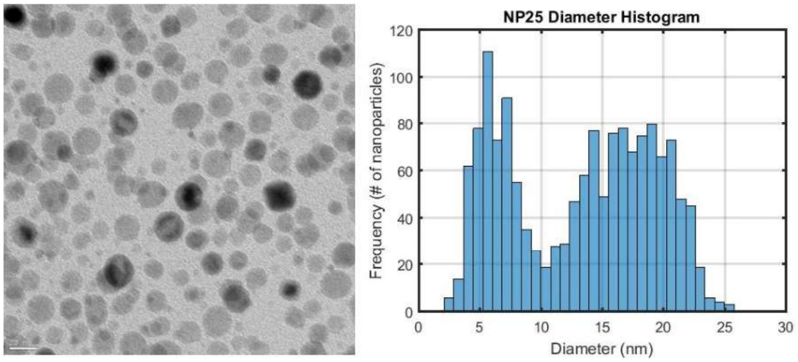

Figure 2.4 TEM image of NP25. Distribution graph of particle diameter is shown next to the image.

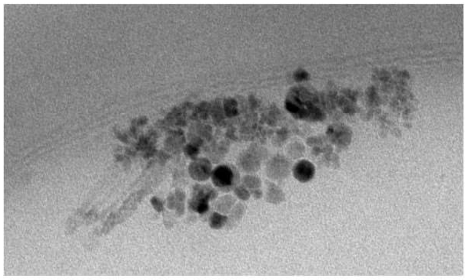

Figure 2.5 TEM image of NP26.

Chapter 3

Synchrotron Experiment and Data

This chapter discusses the experiment performed at the Stanford Linear Accelerator Center (SLAC) synchrotron. In this experiment, the samples of nanoparticles were put through x-ray resonant magnetic scattering (XRMS) which produced scattering images. Details of the XRMS experiment are given, followed by the procedure taken to obtain one-dimensional profiles.

3.1 Synchrotron Experiment

In 2013-2015, the NP16, NP17, and NP18 samples were taken to the Stanford Linear Accelerator Center (SLAC) synchrotron where an experiment using x-ray resonant magnetic scattering (XRMS) was conducted. In XRMS, circulary polarized x-rays are sent through a sample. Clockwise and counterclockwise polarization are referred to as positive and negative polarizations, arbitrarily. As the photon spins interact with the electron spins and as the energy of the x-rays is tuned to resonant L edges, resonant magnetic scattering occurs. The x-rays are scattered due to the spatial variation of the electronic and magnetic structures.

In our experiment, XRMS was performed on each of the samples in the presence of an external magnetic field. A diagram of the experimental setup is shown in Fig. 3.1. As illustrated, scattering

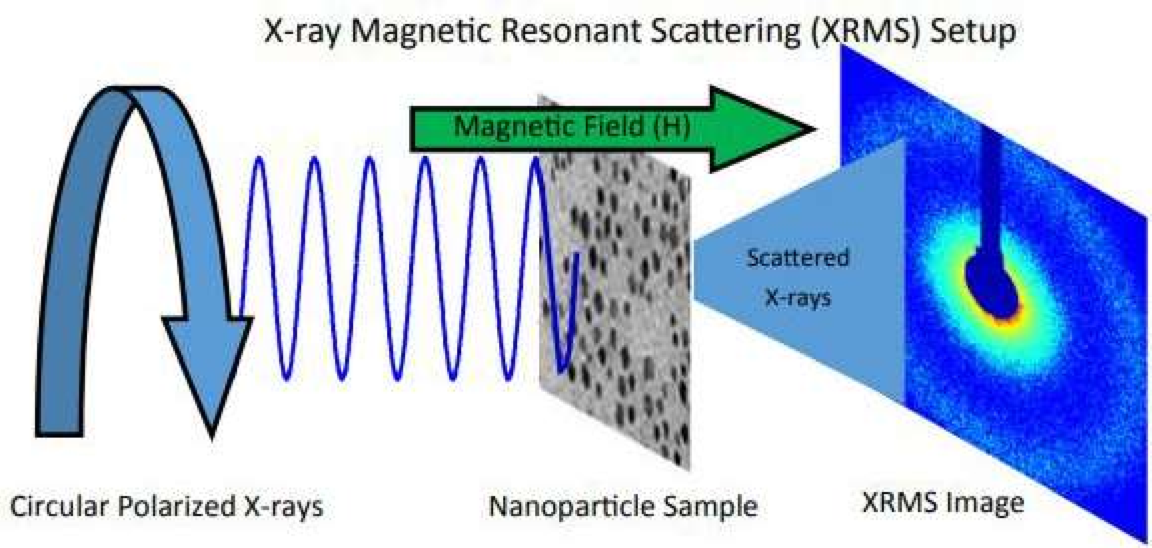

Figure 3.1 Experimental setup of the synchrotron experiment performed at the SLAC synchrotron. Figure taken from Smith's thesis [10].

patterns were captured by a CCD camera. XRMS images were obtained for each sample for both positive and negative polarizations, with field values ranging from -3000 Oe to 3000 Oe, and temperatures ranging from 10 K to 300 K [10].

3.2 Estimation of Interparticle Distance from the XRMS Profiles

In order to extract a magnetic signal from the XRMS data, the two-dimensional scattering images were reduced down to one-dimensional profiles via azimuthal integration. Figure 3.2(a) shows an example of a scattering image, and Fig. 3.2(b) shows its associated representation. The scattering vector is defined as q (the white arrow in Fig. 3.2(a)) and is an inverse distance, typically in units of inverse nanometers. The reduced profile, as shown in Fig. 3.2(b), is then plotted as a function of q. The color on the scattering image represents the intensity of the scattering, blue corresponding to low and red corresponding to high intensity. An important feature in the scattering image is the red ring because this ring's position and width give information about the interparticle distance and correlation length, respectively. Each one-dimensional profile was obtained by first subtracting a background image from the scattering image and removing the region that is covered by the blocker. The dark blue disk at the center is a region masked by a beamstop, to prevent the camera from being damaged by direct x-rays. Angular integration was used to sum a set of concentric rings increasing in radius. Greater detail of obtaining these one-dimensional profiles can be found in Griner's thesis [9] and Smith's thesis [10].

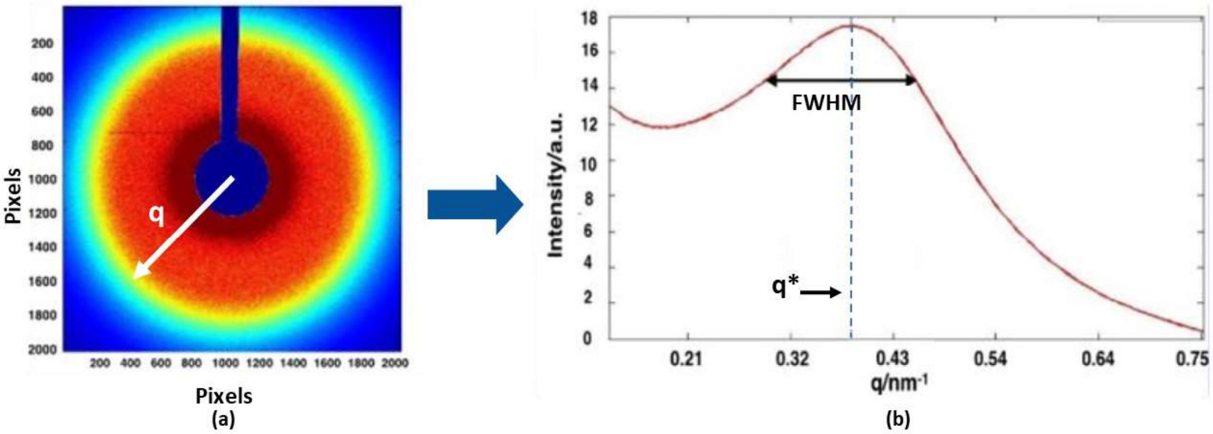

(a) (b)

Figure 3.2 (a) Scattering image from XRMS experiment. (b) One-dimensional representation showing intensity as a function of q obtained by angular integration of a scattering image. Image from Chesnel's submitted paper [12].

The scattering profiles provide information about the interparticle distance and the correlation length. The peak's position is given by q^* as shown in Fig. 3.2(b). The distance from the center of one particle to another, also called the "interparticle distance", is estimated as $d = 2\pi/q^*$. This interparticle distance on the other hand, corresponds to $d = L + 2r$, where L is the separation distance between the particles and r is the average radius of the particles in each sample that was previously determined using TEM imaging. The values of the separation distances and interparticle distances for the samples are given in Table 3.1. These results indicate that the particles in NP18 are packed more closely together than the particles in NP16.

Table 3.1 The radii, separation distances, and interparticle distances of Samples 1-3 and 7-9. Samples 4-6 are not included due to low signal output [9].

Sample	Batch	$2r$ (nm)	L (nm)	d (nm)
1	NP16	11.3 ± 2.5	8.47	19.77
2	NP16	11.3 ± 2.5	9.24	20.54
3	NP16	11.3 ± 2.5	5.27	16.57
7	NP18	5.6 ± 1	0.51	6.11
8	NP18	5.6 ± 1	0.71	6.31
9	NP18	5.6 ± 1	0.58	6.18

The full width half max (FWHM) of the scattering profile intensity peak is shown in Fig. 3.2(b). The inverse of the FWHM gives the correlation length between the particles. A broad peak (large FWHM) represents a short correlation length, meaning that the particles are more dispersed and less ordered. A sharp peak (small FWHM) represents a long correlation length, meaning that particles are more compact and ordered over a longer range [9].

3.3 Magnetic and Dichroic Ratios

The dichroic effect was exploited to extract the magnetic signal from the main charge scattering. As mentioned in the previous section, each sample went through both positive and negative helicities. As can be seen in Fig. 3.3(a), the scattering signal in the positive helicity I_+ is different from the scattering signal in the negative helicity I_-. This result is evidence of a magnetic component in the scattering signal. By taking the difference of the intensities, we can extract the magnetic signal from the charge signal. The intensities from the positive and negative helicities can be used to establish a dichroic ratio. In addition to the standard dichroic ratio, we introduced a magnetic ratio. The dichroic and magnetic ratios are defined below.

This paragraph gives a brief derivation of the dichroic and magnetic ratios. The scattering factor f can be written as

$$f_{\pm} = f_c \pm f_m, \tag{3.1}$$

where the ± sign refers to the helicity of the circularly polarized light, f_c is the charge scattering, and f_m is the magnetic scattering. The scattering amplitude A of a nanoparticle assembly, as a function of the scattering vector q, is given by

$$A_{\pm}(q) = \sum (f_{c,j} \pm f_{m,j}) e^{i\vec{q}.\vec{r}_j} = f_c s_c \pm f_m s_m = A_c \pm A_m. \tag{3.2}$$

The factors s_c and s_m are introduced in Eq. (3.2) as the spatial distributions of the charge and magnetism, respectively, in the nanoparticle assembly. The charge amplitude is then defined as A_c and the magnetic amplitude as A_m. The scattering amplitudes are related to the intensity detected I as:

$$I_{\pm} = |A_{\pm}|^2 = |A_c|^2 \pm (A_c A_m^* + A_m A_c^*) + |A_m|^2. \tag{3.3}$$

Assuming $A_m \ll A_c$, a dichroic ratio R_d and a magnetic ratio R_m are to a first order defined in Eq. (3.4) and Eq. (3.5) as:

$$R_d = \frac{I_+ - I_-}{I_+ + I_-} = \frac{A_c A_m^* + A_m A_c^*}{|A_c|^2 + |A_m|^2} \sim \frac{A_c A_m^* + A_m A_c^*}{|A_c|^2} \propto \frac{s_m}{s_c}, \tag{3.4}$$

$$R_m = \frac{I_+ - I_-}{\sqrt{I_+ + I_-}} = \frac{A_c A_m^* + A_m A_c^*}{\sqrt{|A_c|^2 + |A_m|^2}} \sim \frac{A_c A_m^* + A_m A_c^*}{|A_c|} \propto s_m. \tag{3.5}$$

As can be seen in Eq. (3.4) and Eq. (3.5), R_d is approximately proportional to s_m/s_c and R_m is approximately proportional to s_m [12]. An example of the magnetic and dichroic ratios plotted together is shown in Fig. 3.3(b).

The reason for introducing the magnetic ratio was to access the magnetic signal more directly. The magnetic ratio's magnitude is approximately proportional to the magnetic structure factor s_m, and as the external field value goes negative the magnetic ratio does as well. The position and width

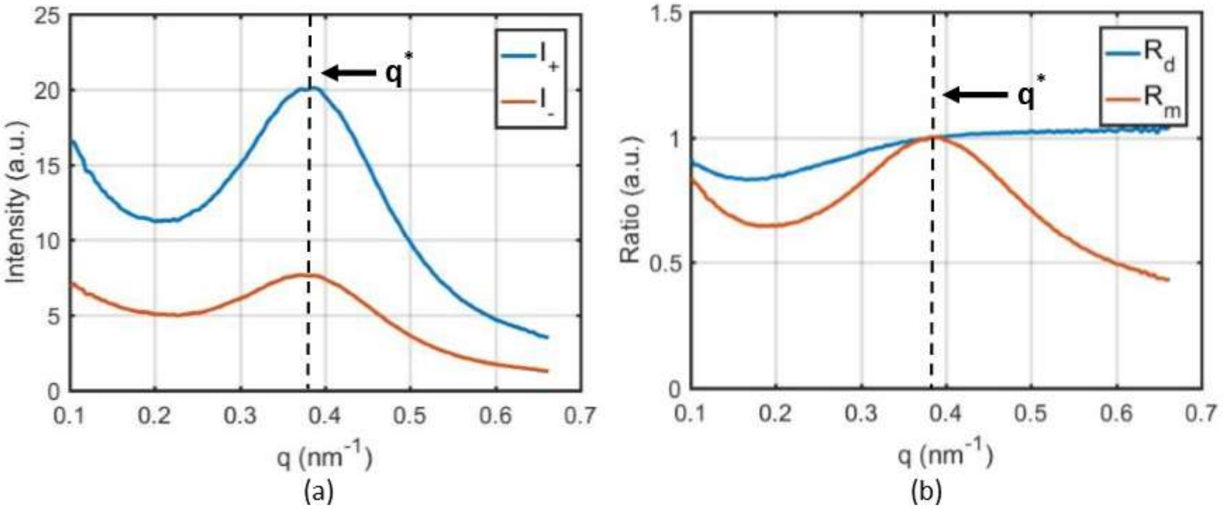

Figure 3.3 (a) Scattered intensity for the positive and negative helicities (I_+ and I_-) as a function of q for Sample 3 at 300 K and 3000 Oe. (b) The resulting dichroic and magnetic ratios (R_d and R_m) as a function of q.

of the peak in the magnetic ratios provide information about the magnetic period and correlation lengths between similarly ordered particles. If many particles are ordered ferromagnetically, we expect the peak of the magnetic ratio to be around the same location, q^*, as the peak for the charge scattering in the XRMS profiles. Particles ordered antiferromagnetically contribute to a peak at around $q^*/2$. As the field value approaches zero, the peak position is expected to shift closer to $q = 0$ as less particles are ferromagnetically ordered and more particles may be ordered antiferromagnetically [10].

Chapter 4

Magnetic Order Modeling of Nanoparticles

This chapter discusses the MATLAB code used to model the experimental data obtained by the methods described in Ch. 3. It covers the previous work done to create the code, as well as the modifications I have made to the code. The different techniques used to obtain a more accurate model are mentioned. Appendix B shows the full MATLAB code used for the model.

4.1 Modeling a Chain of Nanoparticles and Magnetic Ordering

A chain of nanoparticles was modeled by an array of particles with periods defined by the radius of particles and separation between particles. A previous group member, Dallin Smith, created the base MATLAB code which simulates the charge density function and the magnetic density functions associated to a chain of nanoparticles [10]. The particle radius and the separation distance between particles were represented by the variables centerR and centerL, respectively. The chain of nanoparticles typically includes 100 nanoparticles with a distribution of sizes and separation distances.

The magnetic ordering of the particles was modeled by arrays that assign the particles a spin-up or spin-down orientation. Figure 4.1 shows the orientation and periods for nanoparticles that are

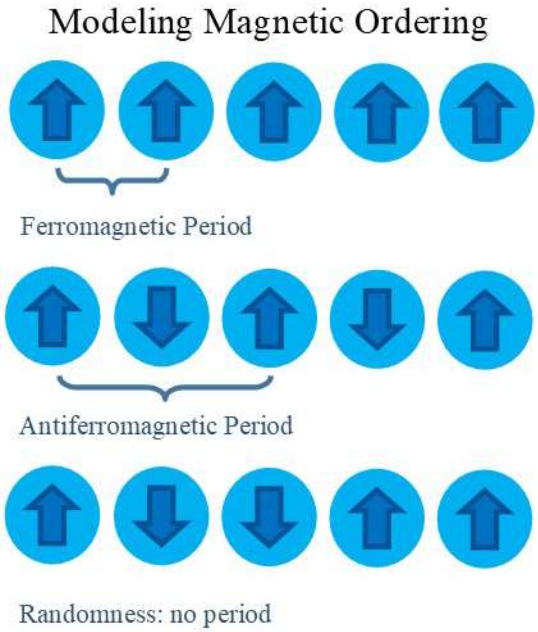

Figure 4.1 Nanoparticle chain for (a) ferromagnetic particles, (b) antiferromagnetic particles and (c) randomly oriented particles.

aligned ferromagnetically, antiferromagnetically, and those that are randomly oriented. As can be seen in the figure, the magnetic period for ferromagnetic particles is equal to the interparticle distance. The magnetic period for the antiferromagnetic particles is twice the interparticle distance. The particles whose spins are oriented randomly do not have a magnetic period since we cannot predict which particles are spin-up versus spin-down.

Spatial Fourier transforms of the magnetic orders were implemented that lead to peaks at certain places in the q space. The Fourier transforms of the ferromagnetic and antiferromagnetic ordering yield a representation of the ordering in the q space. Figure 4.2 shows the Fourier transforms for ferromagnetic and antiferromagnetic ordering. As shown, each ordering has an associated peak in the q space. For the ferromagnetic ordering, the fundamental peak is the one that is located at $q = q^*$, here $q = 1\ \mathrm{nm}^{-1}$. This magnetic peak is located at the same location as the main peak in charge scattering profiles discussed in chapter 3. We note that there is also a peak located at $q = 0$ for the

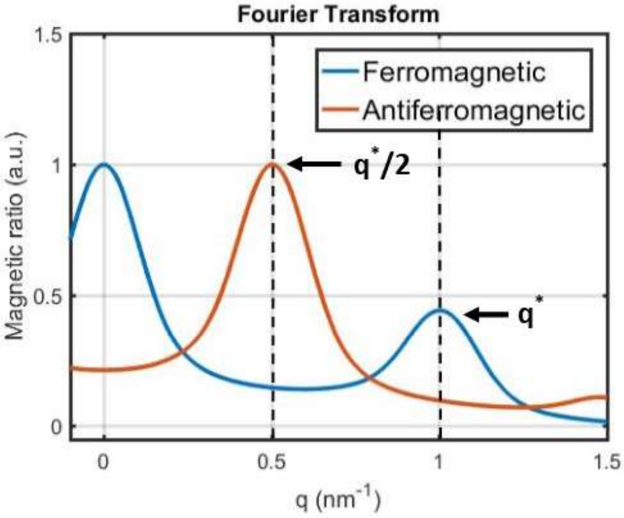

Figure 4.2 Fourier transforms for the different magnetic orders. The ferromagnetic peak occurs at q^* and the antiferromagnetic peak occurs at $q^*/2$. Arbitrary widths have been assigned to the peaks.

ferromagnetic ordering due to the net magnetization it creates. However, this peak can be ignored since in the experiment, this region is blocked by the beamstop. For the antiferromagnetic ordering, the peak occurs at $q = q^*/2$, here $q = 0.5\ \text{nm}^{-1}$, which is halfway between the ferromagnetic peak and $q = 0$. Randomly oriented particles do not produce a peak in the q space because the Fourier transform averages to zero.

Each type of magnetic order was assigned a coefficient to represent a percentage of that contribution in the nanoparticle chain. The coefficients for the ferromagnetic, antiferromagnetic, and random contributions are c1, c2, and c0 respectively. The sum of the coefficients must be equal to one since they represent percentages of the assembly of nanoparticles. For each XRMS run at the SLAC synchrotron, a magnetic field was applied which induced a net magnetization in the nanoparticle assembly. The ferromagnetic ordering is the only ordering that contributes to this magnetization because the spins of the antiferromagnetic and of the randomly aligned particles sum to zero. Thus, the contribution of the ferromagnetic ordering, c1, is predetermined by the magnetization of the sample, which we call M_c. The other coefficients, c2 and c0, must be fit to the experimental data to determine their values. We assume that the three coefficients add up to 1, or 100%. Equations (4.1) and (4.2) show the constraints mentioned above.

$$\mathrm{c1} = \mathrm{M}_c, \tag{4.1}$$

$$\mathrm{c1 + c2 + c0 = 1.} \tag{4.2}$$

The ferromagnetic and antiferromagnetic orders were also assigned sigma values (sig1 and sig2, respectively) to represent the correlation length in the magnetic ordering. This was important in determining how many particles in each order are correlated. The sigma values in the model affect the widths of the peaks in the Fourier transforms. We are thus able to fit the width of the peaks in the one-dimensional profiles from the scattering images by changing the sigma values.

After finding the Fourier transforms of the ferromagnetic and antiferromagnetic orders and creating coefficients to assign percentages to their orderings, the model for the magnetic ratio was defined. This was done by summing the Fourier tranforms with each order multiplied by their respective coefficient. The result was then inserted into Eq. (3.5) for the magnetic ratio introduced in chapter 3. Section 4.2 discusses the modifications that have been made to the code to improve the model.

4.2 Modifications to Previous Model

This section discusses the alterations made to the previous model. It reviews how the changes were implemented and the results of the changes that were made.

4.2.1 Modeling Spatial Distance between Particles

To achieve a more accurate representation, we modified how the code models the spatial distance between the particles. In the previous code, the separation distance between particles and the radii of the particles were set by the same variable in the code. We added another loop to the sequence so that the spacing between the particles is modeled independent of the particle size. This approach creates a more accurate representation of the nanoparticles because the distance between the nanoparticles in our samples is not correlated to their size.

4.2.2 Flattening Technique

We stopped using what was known as the "flattening technique" in order to obtain a more natural fit. The previous model flattened the peak that occurs for the ferromagnetic ordering at $q = 0$ to a constant value. This technique was used to simplify the modeling process since we are more concerned about modeling the ferromagnetic peak due to the magnetic ordering which occur at greater q values. However, we found that we needed to include an additional component to recreate the diffuse scattering centered about $q = 0$. The peak at $q = 0$ is not measured in our scattering experiment due to the beamstop. However, we may see the tail of this diffuse scattering contribution. To create a more natural fit, we created coefficients c7 and sig7 to model the height and width of the peak at $q = 0$, respectively.

4.2.3 Constraining Sigma Values

We constrained the sigma values so that the results of the model have physical meaning. The previous model had unconstrained sigma values or no sigma values, which often led to small sigma values being implemented in the model. A very small sigma value implies a short correlation length. However, by definition, the correlation length cannot be smaller than one magnetic period. We

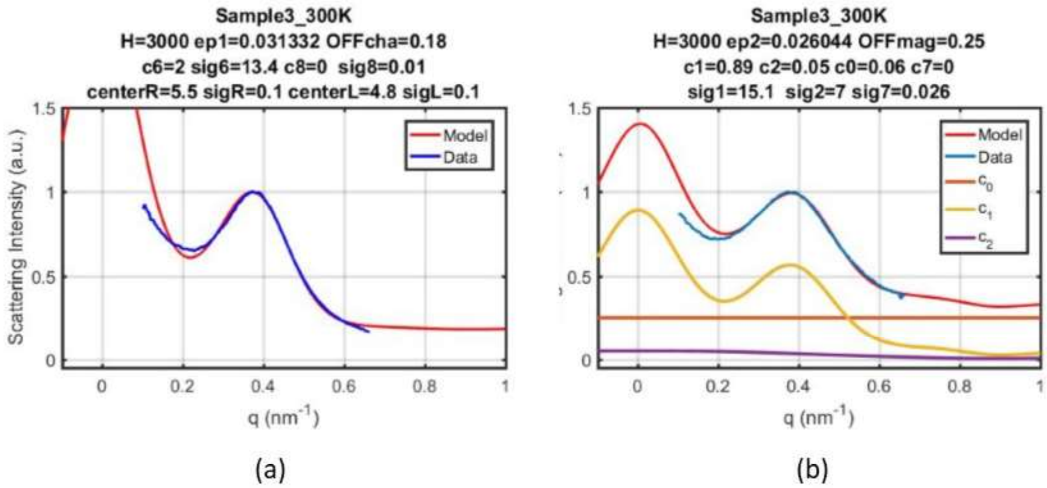

Figure 4.3 Example of a fit for (a) the charge data and (b) the magnetic data.

therefore constrained the sigma values to at least 7 nm for Sample 3 and for Sample 9. This value can be adjusted accordingly depending on the size of the nanoparticles.

4.2.4 Modeling the Magnetic and Dichroic Ratios

We corrected the expressions which model the magnetic and dichroic ratios. These expressions previously contained an approximation that did not account for the imaginary part of the intensity in Eq. (3.3). We included the imaginary part and implemented the equations for the dichroic and magnetic ratios, given by Eq. (3.4) and Eq. (3.5) respectively, without the final approximation displayed in these equations. We then corrected the MATLAB code so that it included the more accurate ratios.

4.2.5 Creating a Global Fit

Since we included the charge contribution in the equations, we needed to model the charge data to achieve a global fit which would include both charge and magnetic fits. To do this, we created a model to fit the charge scattering intensity, which corresponds to $I_+ + I_-$. We assigned a coefficient, c6, and a sigma value, sig6, to model the height and width of the charge scattering peak, respectively. Similarly, the variables c8 and sig8 were implemented to model the height and width of the peak at $q = 0$. We took the Fourier transform of the nanoparticle chain described in section 4.1, before it was assigned a magnetic ordering. We then took the absolute value of the Fourier transform, multiplied it by c6, and normalized it to obtain the model. The model for charge scattering intensity and the model for the magnetic ratio, defined in Eq. 3.5, were used to perform global fits of the data. Figure 4.3 shows an example of a global fit, including a fit of the charge data and a fit of the magnetic data. As seen in the figure, both fits are relatively good, with a low residual (shown by the ep1 and ep2 values at the top of the figure). The ferromagnetic ordering, c1, contributes the most to the model (see Fig.4.3(b)). The global fits for Sample 9 at 300 K and Sample 3 at 300 K and 280 K are shown in Appendix A.

The final goal of these fits is to calculate the percentages of the different magnetic orders as a function of field value. As mentioned in chapter 3, XRMS images were taken for each sample at field values from H = 3000 Oe to H = -3000 Oe. We are interested in how the percentage of each ordering changes as the field value goes from H = 3000 Oe to H = 0 Oe. After we obtain fits for the profiles from H = 3000 Oe to H = 0 Oe, we then create a graph of the coefficients versus the field value. These coefficients maps are shown and discussed in chapter 5.

4.3 Automating the Code using Julia

Instead of manually fitting each graph, we implemented Julia code to optimize the fit. It became very tedious and time-consuming to manually change the variables which have been discussed above, so we decided to automate the code using the programming language, Julia. Dr. Mark Transtrum helped significantly in translating the MATLAB code to Julia code. We used a function which defined the arrays in the same way as the MATLAB code, but instead of assigning the coefficients and sigma values set numbers, they took in variables. We then ran it through an optimized function in which we gave initial parameters. The optimized function then adjusts the parameters until the residual is minimized. We are still currently working on this automation process, but so far our results are close to what we have achieved with the manual fitting. Once we finish automating the code, we expect to obtain results much faster.

Chapter 5

Results and Discussion

This chapter discusses the results found by fitting the data using the MATLAB code presented in the previous chapter. My work focused primarily on accurately fitting the data for Sample 9 at 300 K and Sample 3 at 300 K and 280 K. The following sections present the magnetic ratios and coefficient maps for those samples at various field values. The global fits are shown in Appendix A. The results for each sample are compared to display how the magnetic ordering changes for large versus small particles. Future goals for this project are then mentioned.

5.1 Sample 9 at 300 K

The magnetic ratios from the XRMS profiles for Sample 9 at 300 K indicate a large contribution of ferromagnetic ordering and random contribution. Figure 5.1 shows the normalized magnetic ratios for Sample 9 at 300 K for different magnetic field strengths. As seen in the figure, there is a peak in intensity at $q^* \approx 1$ nm^{-1} corresponding to an average interparticle distance $d = 6.28$ nm, and for lower q values the intensity remains relatively flat. Since there is not evidence of a peak in intensity at $q^*/2$, we expect to see very little antiferromagnetic contribution as the field value decreases. A small antiferromagnetic contribution causes a large random contribution at low field values.

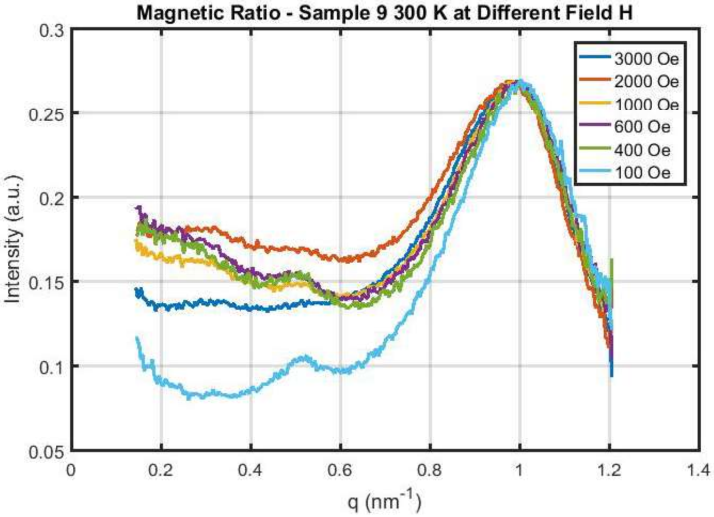

Figure 5.1 Normalized magnetic ratios for all field values of Sample 9 at 300 K.

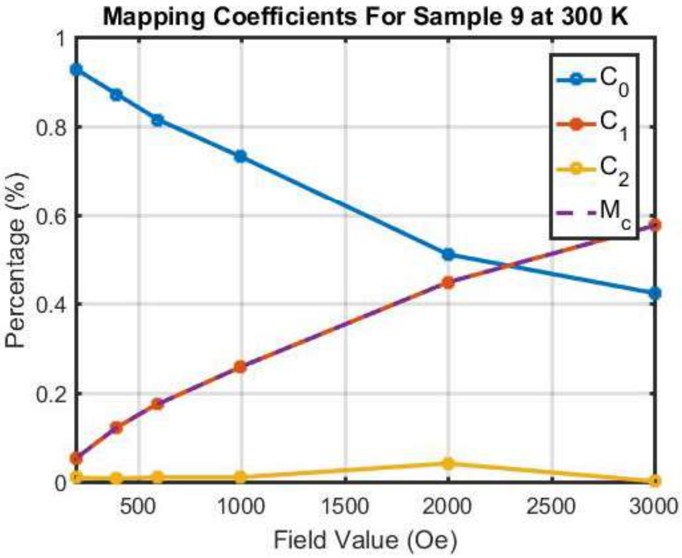

Figure 5.2 Coefficient map for Sample 9 at 300 K. Mostly random contribution occurs as the field value approaches zero.

Similar to the XRMS results for Sample 9 at 300 K, our model indicates mostly ferromagnetic ordering and random contribution as the field value approaches zero. The coefficient map from our model is shown in Fig. 5.2. The percentage of ferromagnetic ordering, labeled as c_1 on the graph, follows the magnetization of the sample (discussed in Sec. 4.1), which is labeled as M_c. This is to be expected since the ferromagnetic ordering is the only ordering contributing to the magnetization in our model. The random contribution, c_0, increases as the field value approaches zero. The antiferromagnetic contribution, c_2, stays consistently lower than about 3%. Thus our model shows a much greater percentage of the particles ordering randomly rather than antiferromagnetically as the field value approaches zero. The results from our model support what we had predicted from the experimental data and confirm the superparamagnetic nature of the nanoparticles.

5.2 Sample 3 at 300 K

The magnetic ratios from the XRMS profiles for Sample 3 at 300 K indicate the presence of antiferromagnetic ordering as the field value approaches zero. The normalized magnetic ratios for Sample 3 at 300 K are shown in Fig. 5.3. The ferromagnetic peak occurs at $q^* = 0.38$ nm^{-1} corresponding to an average interparticle distance $d = 16.53$ nm. At $q^*/2$, a significant change in the intensity occurs, with the formation of a plateau at H = 100 Oe and H = 200 Oe. The flattening and increase in intensity at this location suggest antiferromagnetic ordering; thus, in our model we expect to find a greater percentage of antiferromagnetic ordering for these field values.

My results from the model show that there is some antiferromagnetic ordering and mostly random contribution as the field value approaches zero. Figure 5.4 shows the coefficient map for Sample 3 at 300 K. The percentage of ferromagnetic ordering, c_1, follows the magnetization of the sample, M_c, as it did for Sample 9. The random contribution, c_0, increases as the field value approaches zero. The antiferromagnetic contribution, c_2, increases at H = 100 Oe and H = 200 Oe by 9.5%. Although we expected to see a greater percentage of antiferromagnetic ordering, our results indicate noticeable antiferromagnetic ordering at low field value.

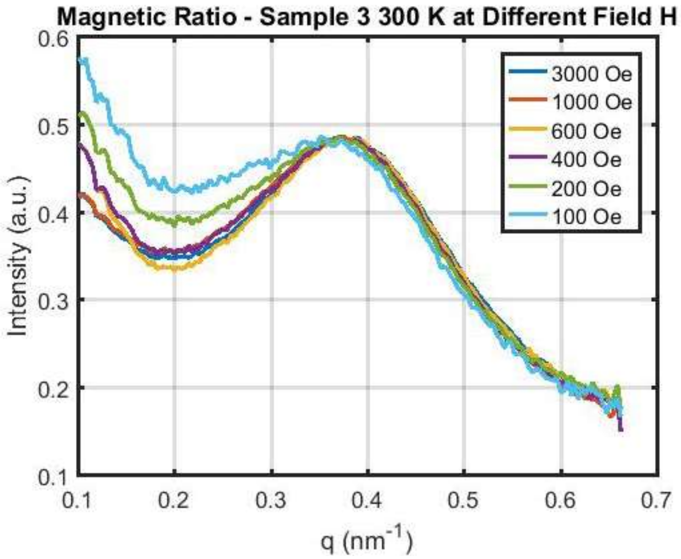

Figure 5.3 Normalized magnetic ratios for all field values of Sample 3 at 300 K. At $q*/2$ the intensity increases for the magnetic ratios of H = 100 Oe and H = 200 Oe. This implies a greater antiferromagnetic contribution at these field values.

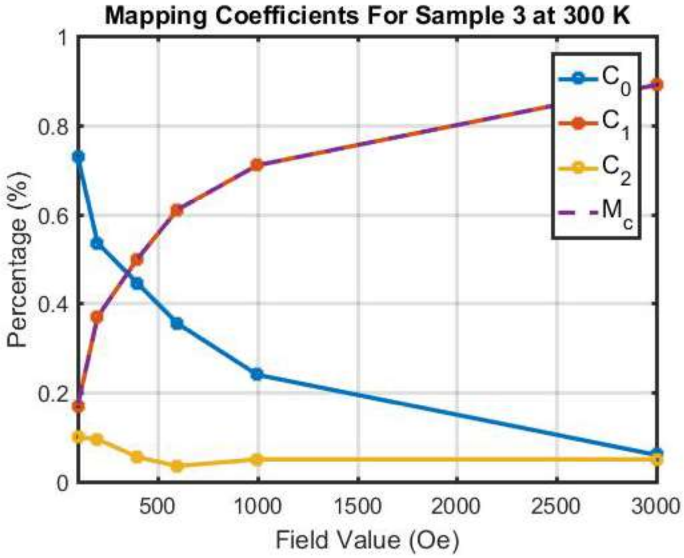

Figure 5.4 Coefficient map for Sample 3 at 300 K. A small increase in the antiferromagnetic contribution is present at H =100 Oe.

5.3 Sample 3 at 280 K

Similar to Sample 3 at 300 K, the magnetic ratios for the XRMS profiles for Sample 3 at 280 K indicate the presence of antiferromagnetic ordering at low field values. As seen in Fig. 5.5, the ferromagnetic peak occurs at the same value as Sample 3 at 300 K. Like at 300 K, the signal at around $q^*/2$ changes significantly with H. Because of this flattening, we expect to see an increase in antiferromagnetic ordering as the field value decreases.

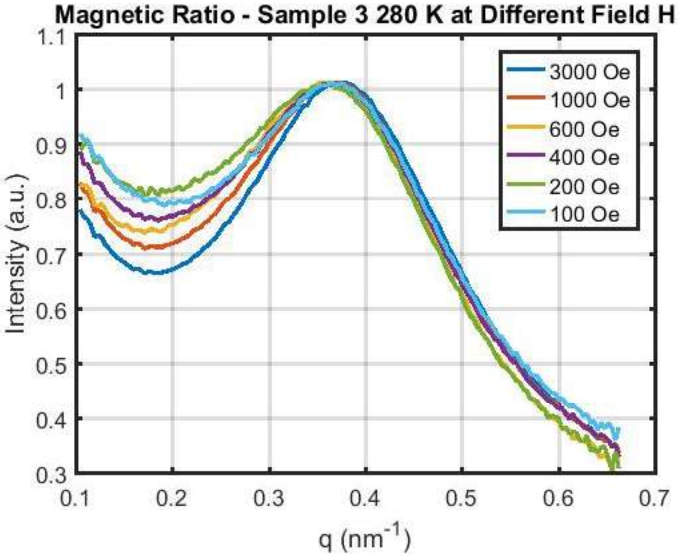

Figure 5.5 Normalized magnetic ratios for all field values of Sample 3 at 280 K. At $q^*/2$ the intensity increases for the magnetic ratio H = 200 Oe, suggesting a significant antiferromagnetic contribution at this field value.

From our model we found that there is a small peak in the antiferromagnetic ordering at 200 Oe but mostly random ordering as the field value decreases. The coefficient map from our model can be seen in Fig. 5.6. The coefficient map shows that the ferromagnetic ordering follows the magnetization and the random contribution increases as the field value decreases. The percentage of antiferromagnetic contribution peaks to 5% at H = 200 Oe. Our model thus suggests noticeable antiferromagnetic contribution at low field value, but mostly random contribution.

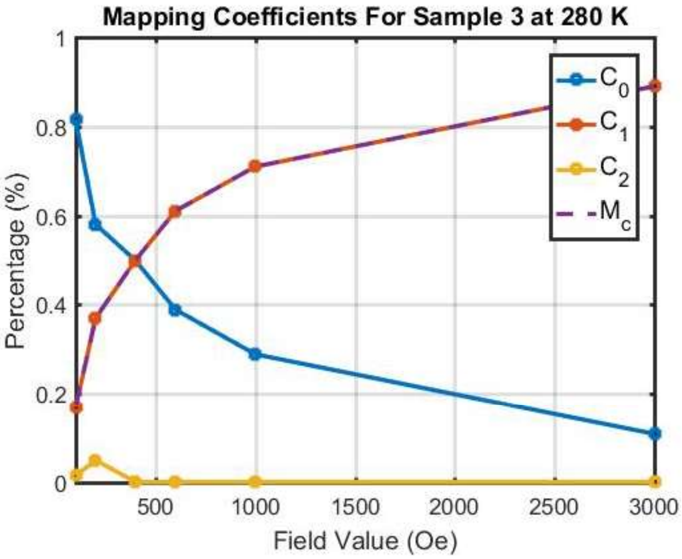

Figure 5.6 Coefficient map for Sample 3 at 280 K. A small peak in the antiferromagnetic contribution is present at H = 200 Oe.

5.4 Discussion of Results

From the XRMS profiles of Sample 3 and Sample 9, we predicted a larger antiferromagnetic contribution for Sample 3 than Sample 9 as the field value decreases. Comparing Fig. 5.1, Fig. 5.3, and Fig. 5.5, it can be seen that the shape of the magnetic ratios for Sample 9 remain unchanged and the shape of the magnetic ratios for Sample 3 flatten and increase as the field value decreases. We had expected to find a greater percentage of antiferromagnetic ordering at low field value for Sample 3 than our model shows, but we did find a larger contribution of antiferromagnetic ordering in Sample 3 than in Sample 9. Thus, the results from our models confirm that there is slightly more antiferromagnetic ordering in the larger particles in Sample 3 than there is in the small particles in Sample 9 at high temperature.

5.5 Conclusion

This paper has discussed how we have determined the magnetic ordering of Sample 9 and Sample 3 at high temperature as a function of field value. Our results show that Sample 3 has slightly more antiferromagnetic ordering for low field value than Sample 9. This indicates that at high temperature the larger nanoparticles show more antiferromagnetic ordering for low field value than the smaller nanoparticles. We have found that by modeling the experimental data we are able to make conclusions regarding the magnetic ordering of the nanoparticles. These results lead to greater understanding of magnetite nanoparticles properties.

5.6 Future Outlook

There is still much to be done in continuation of this project. My study focused primarily on comparing the magnetic ordering for large versus small particles at high temperature. We will need to fit the remaining data for the other samples at low temperature to see how low temperature contributes to the magnetic ordering. Another future goal of this project is to implement error bars for the ordering coefficients to determine the percentage range for each coefficient, which would help us make stronger conclusions. We will also continue optimizing the preparation method of the nanoparticles to achieve even size and distribution to be used for future studies.

Appendix A

Model Fits

Appendix A shows the model fits for Sample 9 at 300 K and Sample 3 at 300 K and 280 K. For each sample, seven global fits were achieved for various field values. Figures A.1 and A.2 display the model fits for Sample 9 at 300 K. Figures A.3 and A.4 display the model fits for Sample 3 at 300 K. Figures A.5 and A.6 display the model fits for Sample 3 at 280 K. The charge (left) and magnetic (right) fits are shown in each figure.

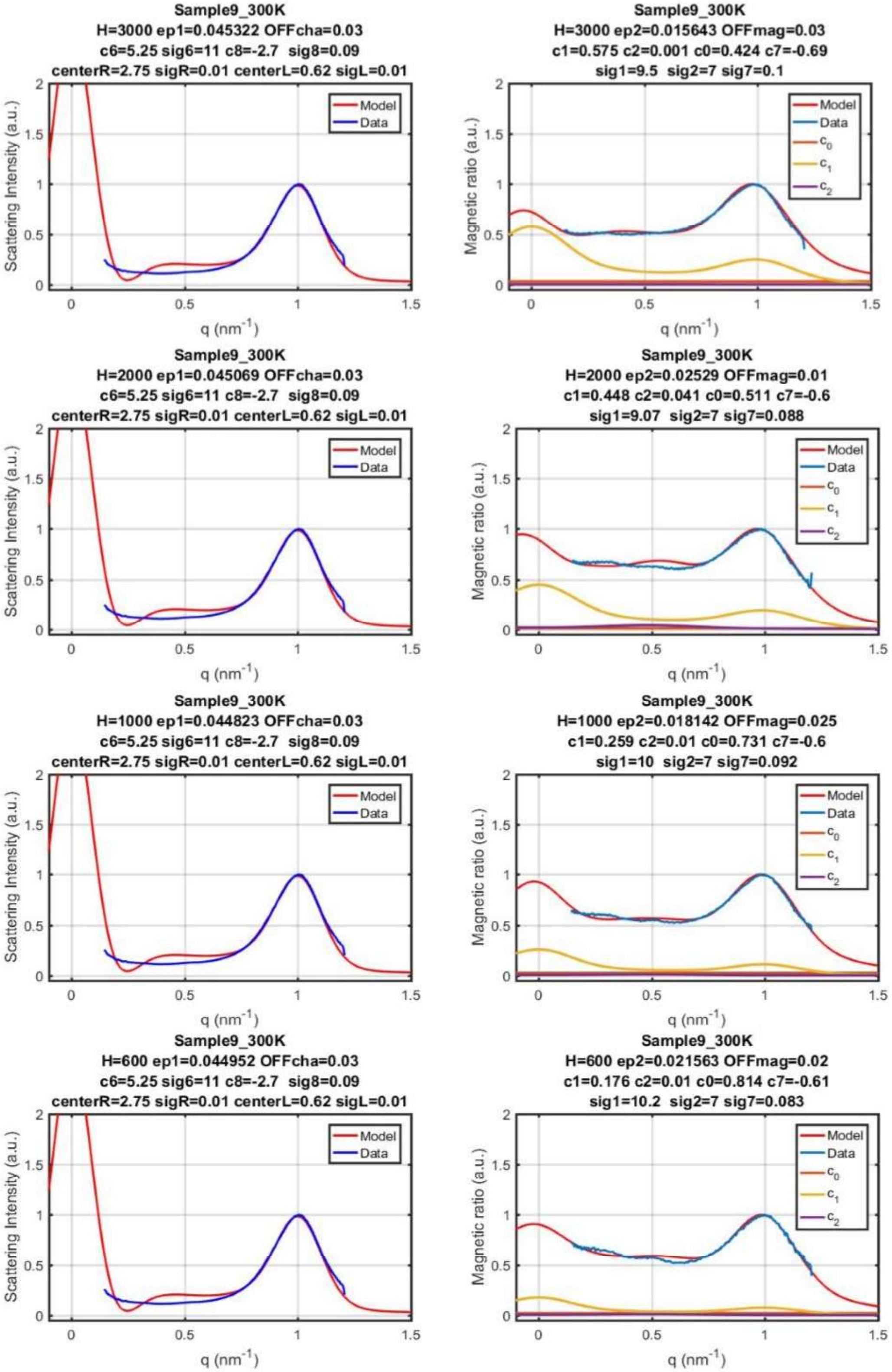

Figure A.1 Model fits for Sample 9 at 300 K and H = 3000, 2000, 1000, and 600 Oe.

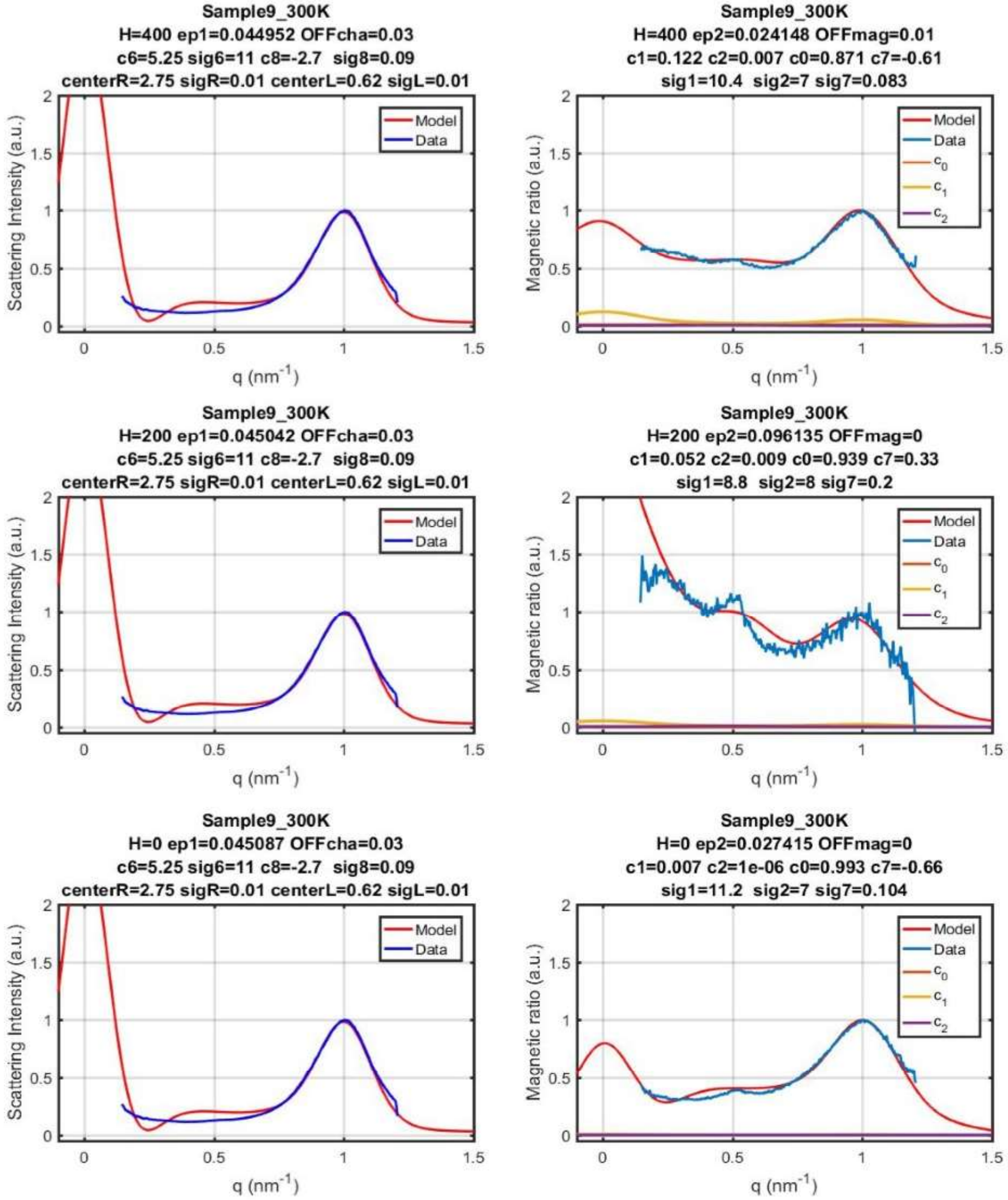

Figure A.2 Model fits for Sample 9 at 300 K and H = 400, 200, and 0 Oe.

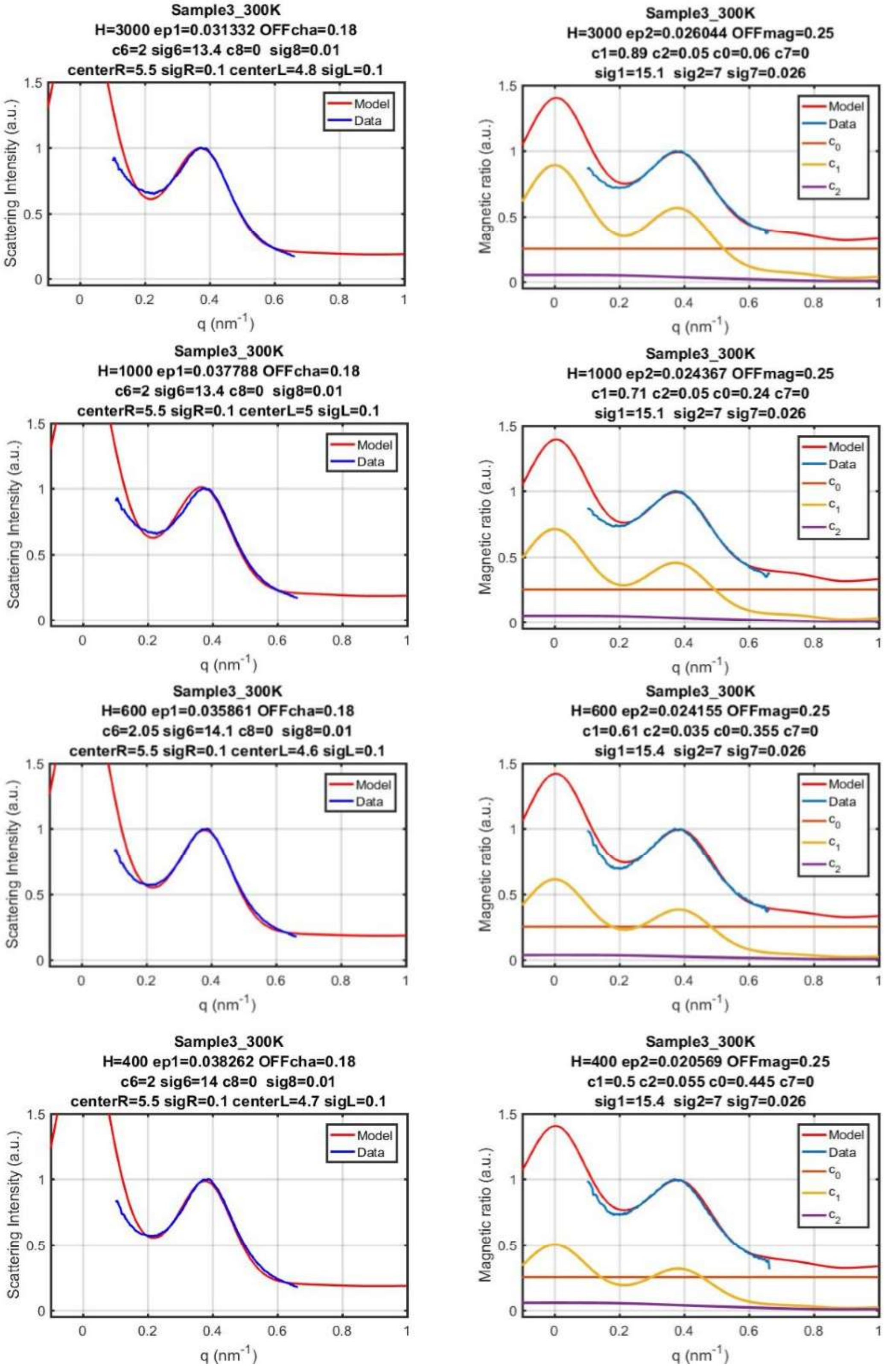

Figure A.3 Model fits for Sample 3 at 300 K and H = 3000, 1000, 600, and 400 Oe.

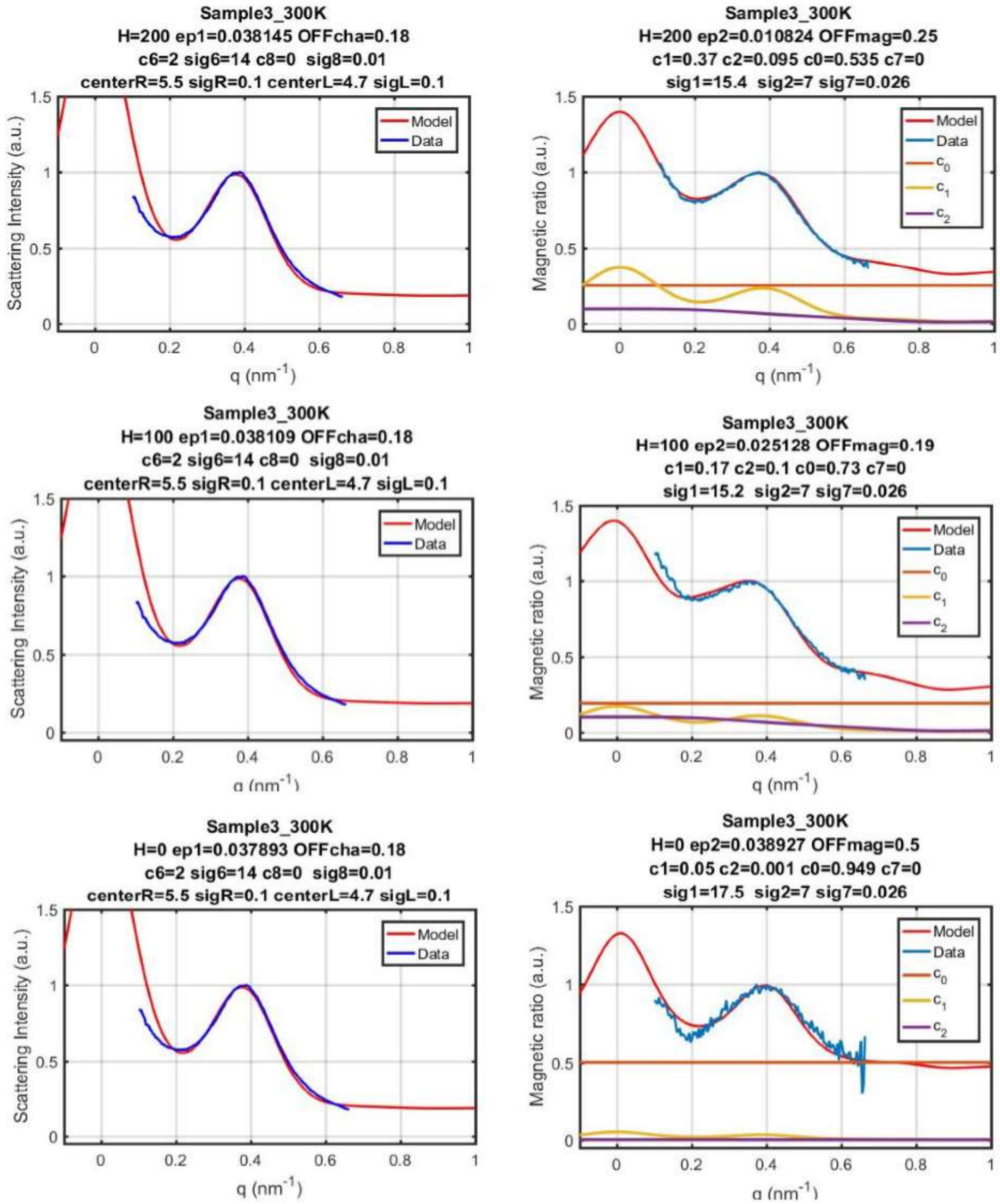

Figure A.4 Model fits for Sample 3 at 300 K and H = 200, 100, and 0 Oe.

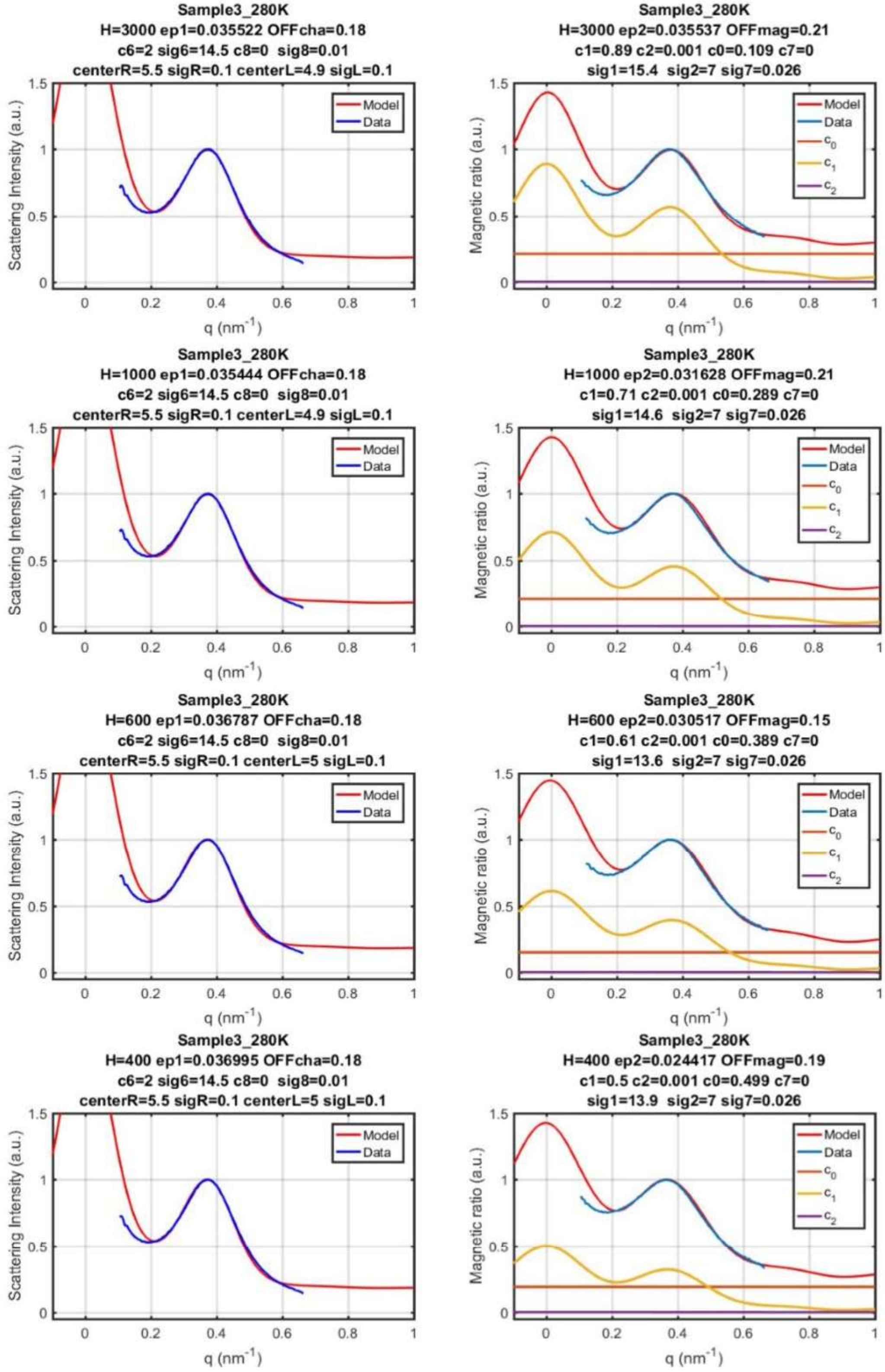
Sample3_280K
H=3000 ep1=0.035522 OFFcha=0.18
c6=2 sig6=14.5 c8=0 sig8=0.01
centerR=5.5 sigR=0.1 centerL=4.9 sigL=0.1

Sample3_280K
H=3000 ep2=0.035537 OFFmag=0.21
c1=0.89 c2=0.001 c0=0.109 c7=0
sig1=15.4 sig2=7 sig7=0.026

Sample3_280K
H=1000 ep1=0.035444 OFFcha=0.18
c6=2 sig6=14.5 c8=0 sig8=0.01
centerR=5.5 sigR=0.1 centerL=4.9 sigL=0.1

Sample3_280K
H=1000 ep2=0.031628 OFFmag=0.21
c1=0.71 c2=0.001 c0=0.289 c7=0
sig1=14.6 sig2=7 sig7=0.026

Sample3_280K
H=600 ep1=0.036787 OFFcha=0.18
c6=2 sig6=14.5 c8=0 sig8=0.01
centerR=5.5 sigR=0.1 centerL=5 sigL=0.1

Sample3_280K
H=600 ep2=0.030517 OFFmag=0.15
c1=0.61 c2=0.001 c0=0.389 c7=0
sig1=13.6 sig2=7 sig7=0.026

Sample3_280K
H=400 ep1=0.036995 OFFcha=0.18
c6=2 sig6=14.5 c8=0 sig8=0.01
centerR=5.5 sigR=0.1 centerL=5 sigL=0.1

Sample3_280K
H=400 ep2=0.024417 OFFmag=0.19
c1=0.5 c2=0.001 c0=0.499 c7=0
sig1=13.9 sig2=7 sig7=0.026

Figure A.5 Model fits for Sample 3 at 280 K and H = 3000, 1000, 600, and 400 Oe.

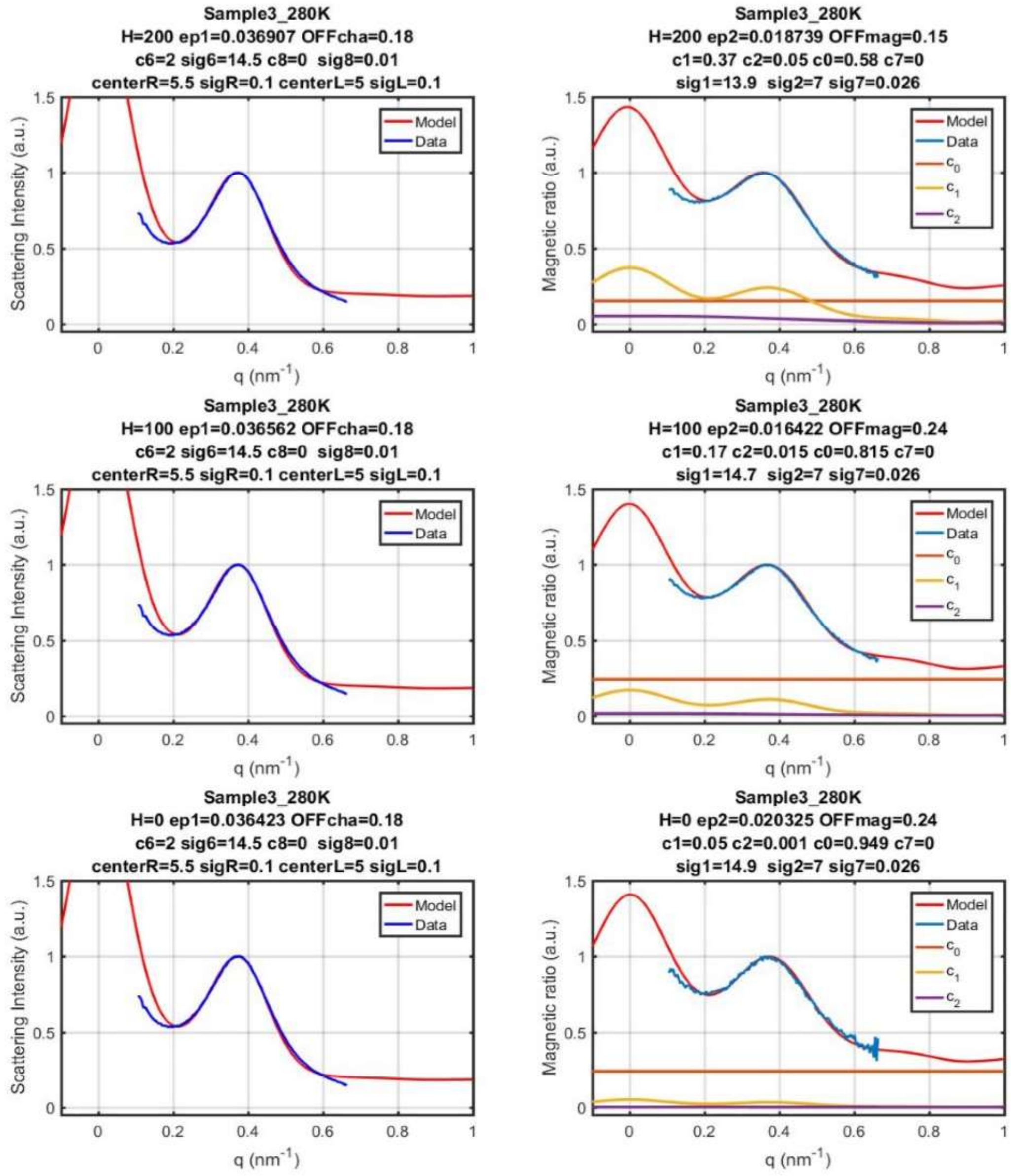

Sample3_280K
H=200 ep1=0.036907 OFFcha=0.18
c6=2 sig6=14.5 c8=0 sig8=0.01
centerR=5.5 sigR=0.1 centerL=5 sigL=0.1

Sample3_280K
H=200 ep2=0.018739 OFFmag=0.15
c1=0.37 c2=0.05 c0=0.58 c7=0
sig1=13.9 sig2=7 sig7=0.026

Sample3_280K
H=100 ep1=0.036562 OFFcha=0.18
c6=2 sig6=14.5 c8=0 sig8=0.01
centerR=5.5 sigR=0.1 centerL=5 sigL=0.1

Sample3_280K
H=100 ep2=0.016422 OFFmag=0.24
c1=0.17 c2=0.015 c0=0.815 c7=0
sig1=14.7 sig2=7 sig7=0.026

Sample3_280K
H=0 ep1=0.036423 OFFcha=0.18
c6=2 sig6=14.5 c8=0 sig8=0.01
centerR=5.5 sigR=0.1 centerL=5 sigL=0.1

Sample3_280K
H=0 ep2=0.020325 OFFmag=0.24
c1=0.05 c2=0.001 c0=0.949 c7=0
sig1=14.9 sig2=7 sig7=0.026

Figure A.6 Model fits for Sample 3 at 280 K and H = 200, 100, and 0 Oe.

Appendix B

MATLAB Code

Appendix B displays the MATLAB code used to import the data, fit the data, and generate the coefficient maps in Sections B.1, B.2, and B.3, respectively.

B.1 Importing Data

```
close all; clear;
%% Import data from spreadsheet
[~, ~, raw1] = xlsread('C:\Users\Brittni\Desktop\Magnetic Ordering of Magnetite NPs\Sample 9 300K Positive\Sample 9 Field 300 K','300K Mag Ratio','A2:H293');
raw1(cellfun(@(x) ~isempty(x) && isnumeric(x) && isnan(x),raw1)) = {''};
[~, ~, raw2] = xlsread('C:\Users\Brittni\Desktop\Magnetic Ordering of Magnetite NPs\Sample 9 300K Positive\Sample 9 Field 300 K','300K Charge (I++I-)','A2:H293');
raw2(cellfun(@(x) ~isempty(x) && isnumeric(x) && isnan(x),raw2)) = {''};
%% Replace non-numeric cells with NaN
R1 = cellfun(@(x) ~isnumeric(x) && ~islogical(x),raw1); % Find non-numeric cells
```

```
raw1(R1) = {NaN}; % Replace non-numeric cells
R2 = cellfun(@(x) ~isnumeric(x) && ~islogical(x),raw2); % Find non-numeric cells
raw2(R2) = {NaN}; % Replace non-numeric cells
%% Create output variable
data1 = reshape([raw1{:}],size(raw1));
data2 = reshape([raw2{:}],size(raw2));
%% Clear temporary variables
clearvars raw1 R1;clearvars raw2 R2;
%% Removing NaN
for j=1:length(data1(1,:))
    for i=1:length(data1(:,1))
        if(isnan(data1(i,j)))
            data1(i,j)=0;
        end
    end
end
for j=1:length(data2(1,:))
    for i=1:length(data2(:,1))
        if(isnan(data2(i,j)))
            data2(i,j)=0;
        end
    end
end
% Separating Data
q=data1(2:end,1);
int1_0=data1(2:end,8);
int1_200=data1(2:end,7);
int1_400=data1(2:end,6);
int1_600=data1(2:end,5);
```

```
int1_1000=data1(2:end,4);
int1_2000=data1(2:end,3);
int1_3000=data1(2:end,2);
q=data2(2:end,1);
int2_0=data2(2:end,8);
int2_200=data2(2:end,7);
int2_400=data2(2:end,6);
int2_600=data2(2:end,5);
int2_1000=data2(2:end,4);
int2_2000=data2(2:end,3);
int2_3000=data2(2:end,2);
save('M_0n.mat','q','int1_0')
save('M_200n.mat','q','int1_200')
save('M_400n.mat','q','int1_400')
save('M_600n.mat','q','int1_600')
save('M_1000n.mat','q','int1_1000')
save('M_2000n.mat','q','int1_2000')
save('M_3000n.mat','q','int1_3000')
save('C_0n.mat','q','int2_0')
save('C_200n.mat','q','int2_200')
save('C_400n.mat','q','int2_400')
save('C_600n.mat','q','int2_600')
save('C_1000n.mat','q','int2_1000')
save('C_2000n.mat','q','int2_2000')
save('C_3000n.mat','q','int2_3000')
M1=load('M_0n');
M2=load('M_200n');
M3=load('M_400n');
M4=load('M_600n');
M5=load('M_1000n');
```

```
M6=load('M_2000n');
M7=load('M_3000n');
C1=load('C_0n');
C2=load('C_200n');
C3=load('C_400n');
C4=load('C_600n');
C5=load('C_1000n');
C6=load('C_2000n');
C7=load('C_3000n');
q1=M1.q;
int1=M1.int1_0;
int2=M2.int1_200;
int3=M3.int1_400;
int4=M4.int1_600;
int5=M5.int1_1000;
int6=M6.int1_2000;
int7=M7.int1_3000;
int21=C1.int2_0;
int22=C2.int2_200;
int23=C3.int2_400;
int24=C4.int2_600;
int25=C5.int2_1000;
int26=C6.int2_2000;
int27=C7.int2_3000;
set(0,'DefaultAxesFontSize',13);
set(0,'DefaultAxesFontWeight','demi')
set(0,'DefaultAxesLineWidth',2);
set(0,'DefaultLineLineWidth',2.5);
figure
```

```
plot(q1,int7,q1,int6/max(int6)*max(int7),q1,int5/max(int5)*max(int7),q1,int4/max(int4)*max(int7),q1,int3/max(int3)*max(int7),q1,int1/max(int1)*max(int7))
title('Magnetic Ratio - Sample 9 300 K at Different Field H')
legend('3000 Oe','2000 Oe','1000 Oe','600 Oe','400 Oe','100 Oe')
xlabel('q (nm^{-1})')
ylabel('Intensity (a.u.)')
grid on
figure
plot(q1,int27,q1,int26/max(int26)*max(int27),q1,int25/max(int25)*max(int27),q1,int24/max(int24)*max(int27),q1,int22/max(int22)*max(int27),q1,int21/max(int21)*max(int27))
title('Scattering Intensity - Sample 9 300 K at Different Field H')
legend('3000 Oe','2000 Oe','1000 Oe','600 Oe','400 Oe','100 Oe')
xlabel('q (nm^{-1})')
ylabel('Intensity (a.u.)')
grid on
```

B.2 Modeling Code

```
clear; close all;
% Experimental parameters
H = 200 ; % Magnetic field- experimental value
VSM = 0.052; % Magnetization- experimental value
fcr = 11; % real part of the charge form factor for Fe3O4
fci = 26 ; % imaginary part of the charge form factor for Fe3O4
% Fitting parameters
N=100; % number of nanoparticles in the chain
pix=10; % number of points to define one period
sets=11; % number of distributions in the mix
```

```
centerL = 0.62; sigmaL=0.01;  % mean value and variance for the spacing L  (unit = nm)
centerR = 2.75; sigmaR=0.01;   % mean value and variance for the particle radius R (unit = nm)
OFFcha = .03 ;% Offset baseline for charge profile
OFFmag = .0 ; % Offset baseline for magnetic ratio profile
c(1)=VSM; % Ferromagnetic contribution
c(2)=.009; % AF contribution
c(3)=0;% Triple contribution (this is no longer implemented in the model)
c(4)=0; % Quadruple contribution (this is no longer implemented in the model)
c(5)= 1-(c(1)+c(2)); % Random contribution
c(6)= 5.25; % Charge
c(7)= .33; % Central q = 0 peak height magnetic
c(8) = -2.7; % Central q = 0 peak height charge

sigma=zeros(1,7); % values for peak widths
sigma0 = 1; % Width of the Gaussian distribution of set averaging.
sigma(1)=8.8; % FERRO
sigma(2)=8; % AF
sigma(3)=7; % Triple (this is no longer implemented in the model)
sigma(4)=7; % Quadruple (this is no longer implemented in the model)
sigma(5)=7; % Random (NO IMPACT because NO PEAK)
sigma(6)=11; % Charge
sigma(7)=0.2; % central q=0 peak in the q space
sigma(8)= 0.09; % central q = 0 peak in the q space
%% Gaussian distribution for charge density function
z(1,:)=linspace(-3,3,sets); % defining the range [-3,3] (arbitrary unit)
zf(1,:)=exp(-z(1,:).^2./(2*sigma0.^2)); % Gaussian function using sigma as variance
%% Charge Density Function
```

```
begL=centerL-sigmaL/2; enL=centerL+sigmaL/2; % Range of L values (beginning and end values)
begR=centerR-sigmaR/2; enR=centerR+sigmaR/2; % Range of R values (beginning and end values)
period=2*centerR+centerL; % calcuation of the period (unit = nm)
x=linspace(0,(period)*N,N*pix); % spatial x scale to define the density profile (unit = nm)
L=linspace(begL,enL,sets); % distribution of L values (equally spaced)
R=linspace(begR,enR,sets); % distribution of R values (equally spaced)
y1=zeros(sets+1,sets+1,N*pix); % Setting a support for density profile function
% Building the density profile function (including all the different sets of values for L and for R)
for k = 1:sets
    for j = 1:sets
    tau= 2*R(k)+L(j);
    for i=1:length(x)
        w = x(i)- tau*floor(x(i)/tau)-R(k); % parameter to define the location within particle (w=0 at the center of particle)
        if abs(w)<= R(k) % condition for being inside the particle of radius R
            y1(k,j,i) = pi*(R(k)^2 - w^2); % Charge density function of spherical particles projected into 1D axis
        else
            y1(k,j,i) = 0; % empty space between particles
        end
    end
    y1(k,sets+1,:)= y1(k,sets+1,:)+zf(1,j)* y1(k,j,:); % Adding all the sets of charge density functions weigthed with the Gaussian zf
    end
    y1(sets+1,sets+1,:)=y1(sets+1,sets+1,:)+zf(1,k)*y1(k,sets+1,:);
```

```
end
y1(sets+1,sets+1,:)=y1(sets+1,sets+1,:)/max(y1(sets+1,sets+1,:)); % averaged charge density profile
%% Magnetic Density Function
y2=zeros(sets+1,sets+1,N*pix); % setting the function for the magnetic density
for j=1:sets
    for i = 1:sets
        h = 1;
        for k = 1:length(y1(1,1,:))-1 % length of y1 = length of x = N*pix
            if y1(i,j,k)== 0
              if y1(i,j,k+1)~= 0
               findp(i,j,h) = k; % vector idenfying the position x (left extremity) of the h_ieth particle in a given set j
               h = h+1;
              end
            end
        end
    % Now, h = last particle
    findp(i,j,h)=2*findp(i,j,h-1)-findp(i,j,h-2); % adding the last particle N + 1 (does not physical meaning)
    end
end
v=ones(5,length(findp(1,1,:))); % defines the different magnetic orders (v(1,i) is FERRO by default)
          for i=1:length(findp(1,1,:))
            if mod(i,2)== 1 % ANTIFERRO order
                v(2,i)= 1;
            else
                v(2,i)= -1;
            end
```

```
         end
         v(5,:)=2*rand([1,length(findp(1,1,:))])-1; % RANDOM order
for s=1:length(v(:,1)) % number of different orders (basically s = 1:5)
    for i = 1:sets
        for j=1:sets
            for f = 1:length(findp(i,j,:))-1
                if findp(i,j,f)~= 0 && findp(i,j,f+1)
                    lens(i,j,1)= f;
                end
            end
            for g = 1:lens(i,j,1)
                spin(i,j,findp(i,j,g):findp(i,j,g+1))= v(s,g); % Building spin density functions (of +1 and -1's)
            end
            for f = 1:length(y1(1,1,:))
                y2(i,j,f) = y1(i,j,f).*spin(i,j,f); % Building the magnetic density fucntion (multiplying the charge density function by the spin function)
                y2(sets+1,sets+1,f)= y2(sets+1,sets+1,f)+ y2(i,j,f)*zf(1,i)*zf(1,j); % Adding all the sets of magnetic density functions weigthed with the Gaussian zf
            end
        end
    end
    y2(sets+1,sets+1,:)=y2(sets+1,sets+1,:)/max(y2(sets+1,sets+1,:));
    y2_flat(:)=y2(sets+1,sets+1,:);
    y3(s,:)=y2_flat; % normalized magnetic density function for each order (s=1:5)
end
%% Convolving by Gaussian distributions to account for limited magnetic
```

```
    correlation lengthes in real space
for a=1:length(y3(:,1))% number of orders (basically a = 1:5)
    zf1(a,:)=exp(-x.^2/(2*sigma(a)^2)); % Gaussian function, unit for sigma =
        nm of variance sigma(a)
    y3(a,:)=y3(a,:).*zf1(a,:); % multiplying the magnetic profile with
        Gaussian distribution (magnetic correlation length)
end
zf1new(1,:,:)=exp(-x.^2/(2*sigma(6)^2)); % Gaussian function for charge, unit
    for sigma = nm
y1(sets+1,sets+1,:)=y1(sets+1,sets+1,:).*zf1new(1,1,:); % this line is causing
     an error because the rhs is 1x1000x1000 and the lhs is 1x1x1000
% If defining the correlation length lambda as the FWHM of the Gaussian
    distribution, lambda ~ 2.35 sigma
% If defining the correlation length lambda as twice FWHM (~foot to foot) of
    the Gaussian distribution, lambda ~ 4.7 sigma
%% Scattering intensity (Fourier Transform)
% Charge scattering term
cha = zeros(1,N*pix);
cha(:)=fftshift(fft(y1(sets+1,sets+1,:),N*pix)); % Fourier Transform of the
    scattering density profile s_c
intC = abs(cha).^2;  % Absolute value squared = amplitude squared of s_c
intC = c(6)*intC/ max(intC) + OFFcha; % Normalizing + offset
% Magnetic scattering term
mag = zeros(6,N*pix);
for a=1:length(y3(:,1))
    mag(a,:)=fftshift(fft(y3(a,:),N*pix)); % Fourier Transform of the magnetic
         density profile s_m
end
t = -length(mag(1,:))/2:1:length(mag(1,:))/2 - 1; % recenters the FT around q
    = 0
```

```
t = t*2*pi/((period)*N); % scales the variable for q = 2pi / d  with proper unit (= nm^-1)
%% Combining the different magnetic orders with weights c and normalizing
mag(5,:)=ones(1,length(mag(1,:)));
for a=1:2 %Only using the F and AF components (random component not included)
    mag(a,:)=mag(a,:)/max(abs(mag(a,:))); % Normalizing each component to 1 before incorporating weight
    mag(6,:)=mag(6,:)+c(a)*mag(a,:); % Adding the FTs of the different magnetic order with respective weights c
end
% Builds the Magnetic Ratio profile
RM = abs((fci*real(cha)+fcr*imag(cha)).*real(mag(6,:))-(fcr*real(cha)-fci*imag(cha)).*imag(mag(6,:)))./abs(cha);
RM(:)= RM(:)/max(RM(:))+ OFFmag;
%% Gaussian function for the central peak at q = 0
x(2,:)=linspace(-3,3,N*pix);
zf1(7,:)= exp(-x(2,:).^2/(2*sigma(7)^2)); % Gaussian function, variance sigma(7) defined in respect to x(2)= [-3,3]
RM = RM + c(7)*zf1(7,:); % Adding the Gaussian peak (located at q = 0) with an amplitude c(7) for the magnetic profile
zf1(8,:) = exp(-x(2,:).^2/(2*sigma(8)^2)); % Gaussian function, variance sigma(8) defined in respect to x(2)= [-3,3]
intC = intC + c(8)*zf1(8,:);% Adding the Gaussian peak (located at q = 0) with an amplitude c(8) for the charge profile
% Normalization using the peak outside q = 0
flat = RM;
flat(1,[length(flat(1,:))/2-50:length(flat(1,:))/2+50])= flat(1,length(flat(1,:))/2+51);
RM = RM/max(flat);
%%Import and normalize the experimental data
```

```
dataC = importdata('C_200n.mat'); % imports the experimental data: charge scattering profile (I+ + I-)
dataM = importdata('M_200n.mat'); % imports the experimental data: magnetic ratio (I+ - I-)/sqrt(I+ + I-)
qC = dataC.q; % loads the experimental q values for charge intensity
EI = dataC.int2_200; % loads the charge scattering intensity
EI=EI/max(EI);
q = dataM.q; % loads the experimental q values for RM
ERM = dataM.int1_200; % loads the experimental intensity RM
ERM = ERM/max(ERM); % normalizes the intensity (for comparison purposes)
%% Residual
for i=1:length(t)
    tfindingBeg(i)=abs(t(i)-q(1));
    a=min(tfindingBeg);
    if(tfindingBeg(i)==a)
        tPlaceBeg=i;
    end
    tfindingEnd(i)=abs(t(i)-q(end));
    b=min(tfindingEnd);
    if(tfindingEnd(i)==b)
        tPlaceEnd=i;
    end
end
t2 = t(tPlaceBeg:tPlaceEnd); % range for the experimental data
% Residual for the charge intensity
model1 = intC(1,tPlaceBeg:tPlaceEnd); % Selected portion of the modeled charge intensity applied to the experimental range
model1 = interp1(t2,model1,q); % Interpolation of the model (to compare with the experimental data at same q values)
ep1 = mean(abs(model1(2:end-2)-EI(2:end-2))); % Residual = abs (model - data)
```

```
er1 = mean((model1(2:end-2)- EI(2:end-2)).^2); % variance = square (model - data)
% Residual for the magnetic ratio
model2 = RM(1,tPlaceBeg:tPlaceEnd); % Selected portion of the modeled magnetic ratio applied to the experimental range
model2 = interp1(t2,model2,q); % Interpolation of the model (to compare with the experimental data at same q values)
ep2 = mean(abs(model2(2:end-2)-ERM(2:end-2))); % Residual = abs (model - data)
er2 = mean((model2(2:end-2)-ERM(2:end-2)).^2); % variance = square (model - data)
%% Visualisation
set(0,'DefaultAxesFontSize',13);
set(0,'DefaultAxesFontWeight','demi')
set(0,'DefaultAxesLineWidth',2);
set(0,'DefaultLineLineWidth',2.5);
figure; plot(t,intC,'r',q,EI,'b','LineWidth',2)
title({['Sample9_300K'],['H=',num2str(H),' ','ep1=',num2str(ep1),' ','OFFcha=',num2str(OFFcha)],['c6=',num2str(c(6)),' ','sig6=',num2str(sigma(6)),' ','c8=',num2str(c(8)),' ','sig8=',num2str(sigma(8))],['centerR=',num2str(centerR),' ','sigR=',num2str(sigmaR),' ','centerL=',num2str(centerL),' ','sigL=',num2str(sigmaL)]},'interpreter','none')
xlabel('q (nm^{-1})')
ylabel('Scattering Intensity (a.u.)')
legend('Model','Data')
xlim([-.1 1.5])
ylim([-0.05 2])
grid on
figure
skip=1;
plot(t(1:skip:end),RM(1:skip:end),'r',q(1:skip:end),ERM(1:skip:end),'Linewidth
```

```
',2)
hold on
plot(t,OFFmag*abs(mag(5,:)),t,c(1)*abs(mag(1,:)),t,c(2)*abs(mag(2,:)))
title({['Sample9_300K'],['H=',num2str(H),' ','ep2=',num2str(ep2),' ','OFFmag=',num2str(OFFmag)],['c1=',num2str(c(1)),' ','c2=',num2str(c(2)),' ','c0=',num2str(c(5)),' ','c7=',num2str(c(7))],['sig1=',num2str(sigma(1)),' ','sig2=',num2str(sigma(2)),' ','sig7=',num2str(sigma(7))]},'interpreter','none')
xlabel('q (nm^{-1})')
ylabel('Magnetic ratio (a.u.)')
legend('Model','Data','c_0','c_1','c_2')
xlim([-.1 1.5])
ylim([-0.05 2])
grid on
```

B.3 Generating Coefficient Maps

```
clear; close all; %plotting c values
c1=[.575,.448,.259,.176,.122,.052,.007];
c2=[.001,.041,.01,.01,.007,.009,1e-6];
c5=[.424,.511,.731,.814,.871,.928,.993];
M= [.575,.448,.259,.176,.122,.052,.007];
for a=1:length(c1)
    Mc(a)=c1(a);
end
x=[3000,2000,1000,600,400,200,0];
set(0,'DefaultAxesFontSize',13);
set(0,'DefaultAxesFontWeight','demi')
set(0,'DefaultAxesLineWidth',2);
set(0,'DefaultLineLineWidth',2.5);
```

```
figure;
plot(x,c5,'-s',x,c1,'-s',x,c2,'-s',x,Mc,'--')
hh=legend('C_{0}','C_{1}','C_{2}','M_{c}');
set(hh,'Fontsize',14);
xlabel('Field Value (Oe)')
ylabel('Percentage (%)')
title('Mapping Coefficients For Sample 9 at 300 K')
grid on
```

Bibliography

[1] T. L. Doane and C. Burda, "The unique role of nanoparticles in nanomedicine: imaging, drug delivery and therapy," Chemical Society Reviews **41,** 2885–2911 (2012).

[2] C.-N. Shauo, C.-G. Chao, T. M. Wu, and H.-J. Shy, "Magnetic and optical properties of isolated magnetite nanocrystals," Materials Transactions **48,** 1143–1148 (2007).

[3] D.-Y. Kim, A. Kadam, S. Shinde, R. G. Saratale, J. Patra, and G. Ghodake, "Recent developments in nanotechnology transforming the agricultural sector: a transition replete with opportunities," Journal of the science of food and agriculture **98,** 849–864 (2018).

[4] S. M. Moghimi, A. C. Hunter, and J. C. Murray, "Nanomedicine: current status and future prospects," Faseb Journal **19,** 311–330 (2005).

[5] N. A. Frey, S. Peng, K. Cheng, and S. Sun, "Magnetic nanoparticles: synthesis, functionalization, and applications in bioimaging and magnetic energy storage," Chemical Society Reviews **38,** 2532–2542 (2009).

[6] Banerjee, S. K., Moskowitz, and B. M., in *Magnetite Biomineralization and Magnetoreception in Organisms: A New Biomagnetism*, J. L. Kirschvink, D. S. Jones, and B. J. MacFadden, eds., (Springer US, Boston, MA, 1985), pp. 17–41.

[7] Y. P. Cai *et al.*, “Orbital and spin moments of 5 to 11 nm Fe3O4 nanoparticles measured via x-ray magnetic circular dichroism,” Journal of Applied Physics **115,** 17B537 (2014).

[8] K. Chesnel, M. Trevino, Y. Cai, J. M. Hancock, S. J. Smith, and R. G. Harrison, “Particle size effects on the magnetic behaviour of 5 to 11 nm Fe 3 O 4 nanoparticles coated with oleic acid,” Journal of Physics: Conference Series **521,** 012004 (2014).

[9] D. Griner and K. Chesnel, “Study of Magnetite Nanoparticle Assemblies Using X-ray Resonance Magnetic Scattering (XRMS),” Senior Thesis (Brigham Young University, Provo, UT, 2016).

[10] D. Smith and K. Chesnel, “X-ray Studies and Magnetic Ordering Modeling of Chains of Magnetite Nanoparticles,” Senior Thesis (Brigham Young University, Provo, UT, 2016).

[11] J. Park, K. J. An, Y. S. Hwang, J. G. Park, H. J. Noh, J. Y. Kim, J. H. Park, N. M. Hwang, and T. Hyeon, “Ultra-large-scale syntheses of monodisperse nanocrystals,” Nature Materials **3,** 891–895 (2004).

[12] K. Chesnel, D. Griner, Y. Cai, M. Trevino, K. Jones, R. G. Harrison, T. Wang, T. Liu, E. Jal, and A. Reid, “Unraveling magnetic ordering in Fe3O4 nanoparticle assemblies via x-rays,” Manuscript submitted for publication .

Index

Antiferromagnetic Ordering, 4

Coefficient Map
  Sample 3 280K, 30
  Sample 3 300K, 28
  Sample 9 300K, 26

Ferromagnetic Ordering, 3
Flattening Technique, 21
Fourier Transform, 18–20, 23

Global Fits, 23
Griner
  Previous Work, 4, 6, 9, 13, 14

Julia Code
  Code Automation, 23

Magnetic Ordering, 2, 5, 16, 17, 19, 25, 31
Magnetite Nanoparticles
  Applications, 1
  Fabrication, 6, 7

Nanoparticle Chain, 17
Nanoparticle Period, 18

Ratios
  Dichroic, 4, 15
  Magnetic, 4, 15, 20

Smith
  Previous Work, 4, 12, 13, 16, 17
Stanford Linear Accelerator Center
  Synchrotron, 4, 11, 12, 19
Superparamagnetism, 3

Transmission Electron Miscroscopy, 8

X-ray Resonant Magnetic Scattering, 11